System Identification and Adaptive Compensation of Friction in Manufacturing Automation Systems

by

Mustafa Hakan Turhan

A thesis
presented to the University of Waterloo
in fulfillment of the
thesis requirement for the degree of
Master of Applied Science
in
Mechanical Engineering

Waterloo, Ontario, Canada, 2013

I hereby declare that I am the sole author of this thesis. This is a true copy of the thesis, including any required final revisions, as accepted by my examiners.

I understand that my thesis may be made electronically available to the public.

Abstract

Industrial demands for more efficient machine tool systems have been significantly increased. In order to obtain high performance machine tool systems, researchers are focused on enhancing functioning of various components of machine tool systems. Feed drives are important component of the most of machine tool systems such as computer numerical control (CNC) machines for achieving desirable performance. An essential research stream of current interest aiming enhancement of feed drive performance is construction of control methods that help to decrease tool positioning errors in the system. An effective approach for mitigation or reduction of positioning errors is modeling, identifying, and compensating friction in appropriate manner. In addition, accurate modeling of feed drive systems is essential in elimination of these positioning errors. In this thesis, the precision control of feed drives is studied using several different control methods. Firstly, the feed drive type that has common use in machine tools is chosen to be main focus for this research, namely ball screw drive. Different dynamic models of ball screw drive are shown in detail. In addition, some of the nonlinearities that affect ball screw dynamics such as friction affects are discussed. Friction modeling needs to be performed realistically and accurately in order to design an effective compensator to cancel friction effects. In general, the friction models are divided into two categories; classic (static) and dynamic friction models. In this thesis, we present details of these models and derive linear parametrization of the key ones. Based on the derived linear parametric models, we design a least-squares on-line friction estimator and adaptive friction compensation scheme. The performance of these designs are verified via simulation and real-time experimental tests. Noting that the parameters of the base rigid body model, i.e., inertia and viscosity constants, need to be known precisely for effective high precision control tasks, including the aforementioned adaptive schemes. The second part of the thesis focuses on off-line identification of these key base model parameters. In this part, we present a real-life case study on identification of plant and built-in controller parameters and a simulator design based on this identification for a grinding CNC machine used in a gear manufacturing company.

Acknowledgements

I would like to express my sincere gratitude to my supervisor, Dr. Baris Fidan for the guidence and support he has provided throughout my graduate studies. This graduate study could not been completed without his help.

Also, I would like to express my greatest appreciation to Dr. Kaan Erkorkmaz for his advise and knowledge he has provided.

I would also like to thank Samet Guler, Yasin Hosseinkhani and Ahmet Okyay for their endless support. In addition, I want to thank Ivan Chan for his valuable collaboration during NSERC project.

I want to thank Ontario Drive-Gear (ODG) company staff for the knowledge they provided and kindness they showed. Especially, I would like to express my gratitude to Jamie McPherson and Bob Reiter for their continuous support.

I would like to thank to Dr. Soo Jeon and Dr. Eihab Abdel-Rahman for the feedback they have given.

I would like to gratefully acknowledge the financial support of the National Education Ministry of Turkey during my graduate studies.

Above all, I would like thank God for helping me to overcome all problems I confronted and making everything possible for me.

To my family

Table of Contents

List of Tables

List of Figures

Chapter 1

Introduction

Computer numerical control (CNC) systems are widely used in various industrial branches such as manufacturing, automotive, and aerospace industries. CNC systems typically consists of mechanical, CNC unit and power electronic. Some of the components of mechanical unit are beds, columns and feed drive systems [1]. In general, there are two types of feed drive systems used for motion delivery purposes; direct(linear) drives and ball screw drives. The significantly growing demand for improving existing precision of materials has drawn many researchers attention into the field of precision control of feed drives. Dynamic modeling holds a crucial place during examining precision of feed drive systems and it can be constructed in different ways ranging from simple rigid body dynamic to more complicated models. Simple rigid body model includes Coulomb friction, affects of inertia and viscous friction. More complicated models are built by covering different internal and external interferences such as cutting forces, torque ripples, and nonlinear friction forces.

Friction has nonlinear affects in machine tools. It, in all drive systems, affects positioning of end-effectors and tools and cause tracking errors. Well established friction models and compensator design based on these models will reduce such errors. In order to investigate characteristics of friction effects, feed drive motion is divided into two regimes; namely pre sliding and sliding regimes. Friction is a function of displacement in presliding regime and function of velocity in sliding regime. While some of the friction models show sliding regime characteristics only, some of them demonstrate both regime behaviors. Generally, classical models [2], [3] , which are in the form of combination of Coulomb, viscous and static friction effects, represent the behavior only in the sliding regime. On the other hand, most of the more recently developed dynamical models characterize both regimes [4], [5], [6]. In Chapter 2, friction phenomena are investigated and mostly used friction models are given. Some of the advantages and disadvantages of these friction models

are discussed.

Compensating friction force and reducing tracking errors due to friction are important components of an effective high precision feed drive control design. In order to reduce friction effects, classical feedback controllers such as P,PI and PID controller or more complicated dither, sliding mode controllers are used [7]. These controllers generally do not require a precise and detailed plant model, however, they can reduce friction effects up to some limited work range. Therefore, in addition to such control techniques, different model based compensating techniques are proposed in the literature and used with feedback controllers [3], [8], [9]. In many studies, model based friction identification methods are performed off-line by processing experimental data. Such data allow identification of friction force parameters for limited motion time. However, friction force parameters can change through time. Online estimation of friction parameters is used in order to overcome this problem [10], [11]. In Chapter 3, we derive linear parametric forms of the two widely used friction models, construct adaptive friction compensation scheme, and design a least-squares on-line friction estimator. Afterwards, we implement these designs in the both real-time experiments and simulations.

For various control tasks such as above mentioned adaptive method, identifying rigid body model parameters, i.e., viscous damping constant and inertia affects accurately is a crucial step. In Chapter 4, identification of these parameters are discussed. Practical real-life case study on finding rigid body model parameters for grinding machine in a gear manufacturing company is also explained.

In Chapter 5, our results are summarized and discussed qualitatively. The near future research plans following this work are also presented.

Chapter 2

Background

2.1 Precision Control of Manufacturing Automation Systems

In order to build high performance computer numerical control (CNC) systems, accurate identification and modeling of feed drives is an important step [3]. High fidelity of the feed drive model used in control design enhances the accuracy and disturbance rejection performance of the design [12]. Dynamic modeling of feed drives typically involves inclusion of different nonlinear effects such as vibration and friction. More simplistic feed drive models include Coulomb friction, inertia and viscous damping effects [13]. In this chapter, the base models that are commonly used for ball screw driven systems are presented. Moreover, friction phenomena and some of the friction models that are used in literature are reviewed.

2.1.1 The Base Linear Model of Ball Screw Drives

In the ball screw drive, flexibilities arise from screw-nut interaction, screw shaft and bearings. In order to obtain high precision dynamic tracking, flexibilities of these sources need to be taken into account. In addition to appropriate physical structural design in ball screw drive system, the negative effects of such flexibilities can be avoided via accurate mathematical modeling and adaptive cancellation as well [14]. As it will be explained below, rigid body model is used to identify low frequency range behavior of the system. Beyond certain frequency range, there occur structural vibrations. Flexible drive models

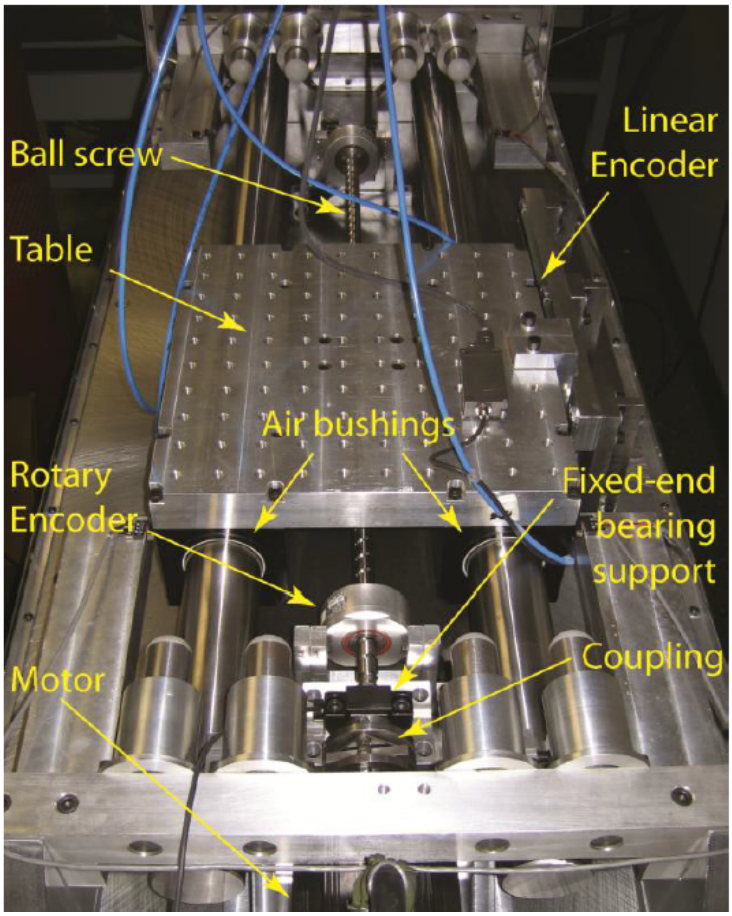

Figure 2.1: Ball screw setup.

that include flexibilities are found useful for identifying and compensating these structural vibrations. However, for ease of control design, rigid body model is taken into account in this study.

Flexible Drive Model: Consider the physical model diagram of the ball-screw drive depicted in Figure 2.2 and the flexible model scheme in Figure 2.3. Here, we model the disturbance due to rotating discrepancies as a friction force $d_1 = F_f$. Rotational friction disturbance is caused by encoder, support ball bearings, nut assembly, and the motor's internal bearings [12]. It should be noted that linear guideways friction is annihilated because of the air bushing use, represented by d_2. x_1 and x_2 represent the ball screw rotational and table linear displacements. The equivalent control signal is u. In addition,

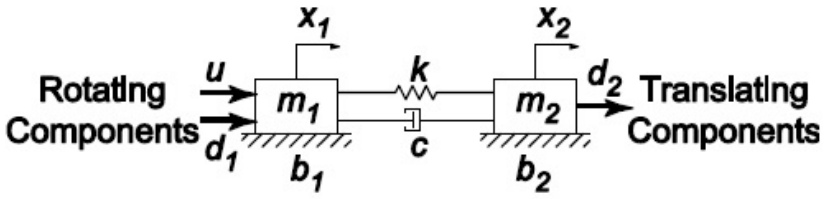

Figure 2.2: Ball screw drive model representation [13].

b_1 represents the viscous friction in the rotary bearings and b_2 shows the viscous friction in the linear guideways. c is the damping coefficient and k is the total stiffness of the ball screw drive system. Total stiffness is combination of the fixed bearing, the nut, and the torsional-axial stiffnesses of the screw. Rotational and translational inertias are represented by m_1 and m_2, respectively. The equations of motion can be written as

$$\begin{aligned} m_1\ddot{x}_1 &= -b_1\dot{x}_1 + k(x_2 - x_1) + c(\dot{x}_2 - \dot{x}_1) + u + d_1 \\ m_2\ddot{x}_2 &= -b_2\dot{x}_2 + k(x_1 - x_2) + c(\dot{x}_1 - \dot{x}_2) + d_2 \end{aligned} \tag{2.1}$$

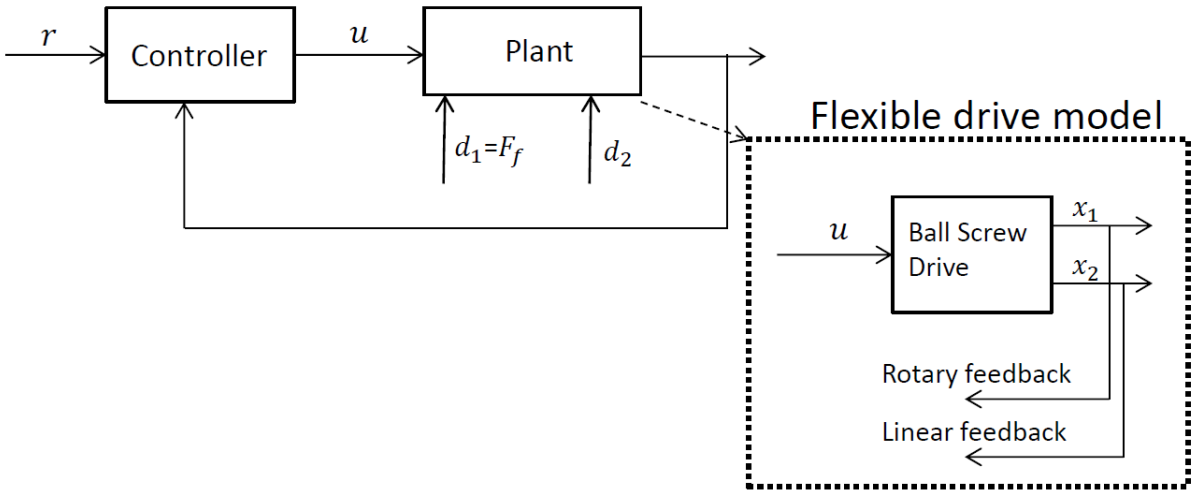

Figure 2.3: Flexible model scheme: with flexibilities.

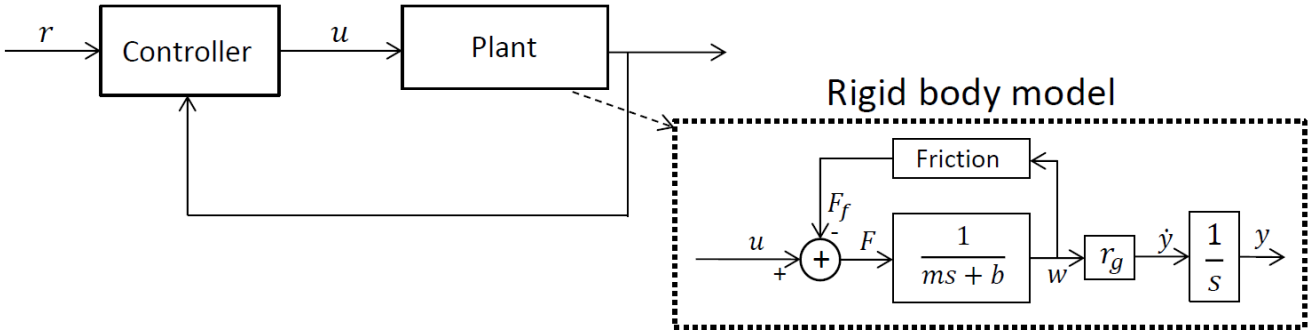

Figure 2.4: Rigid body scheme: without flexibilities.

Rigid Body Model:

Rigid body model derived considering the total inertia as sum of rotational and translational inertia components ($m_1+m_2 = m$). Normally, basic rigid body model is combination of Coulomb friction, viscous damping and inertia effects. Denoting the general friction force by F_f, from the Newton's second law of motion, the equation of motion is

$$m\ddot{y} = -b\dot{y} - F_f + u \tag{2.2}$$

The corresponding space equations can be written as

$$\dot{x}_1 = r_g x_2$$

$$\dot{x}_2 = (-b/m)x_2 + (1/m)F$$

where x_1 and x_2 represent the linear displacement (y) and the angular velocity (w), respectively. b is the viscous friction coefficient and m is the mass of the system. $F = u - F_f$ represents the total force that applied to the plant (Figure 2.4).

2.1.2 Nonlinear Friction Models

The main source of disturbance, causing positioning errors during motion, is friction for the axis control applications. Especially, in the sharp corners or circular arc quadrants, the friction based disturbance causes some tracking error jumps during the motion reversals. Accurate identification of friction characteristic helps to reduce these positioning errors.

Friction characteristic can be better described by considering different regimes: (i) static friction or pre sliding regime, (ii) boundary lubrication regime, (iii) partial fluid lubrication regime and (iv) full fluid lubrication or sliding regime [2].

(i) Static friction or pre sliding regime: In this regime, static friction between contacts acts like a spring. There is displacement until breakaway occurs. After that, junctions break and sliding begins (Figure 2.5).

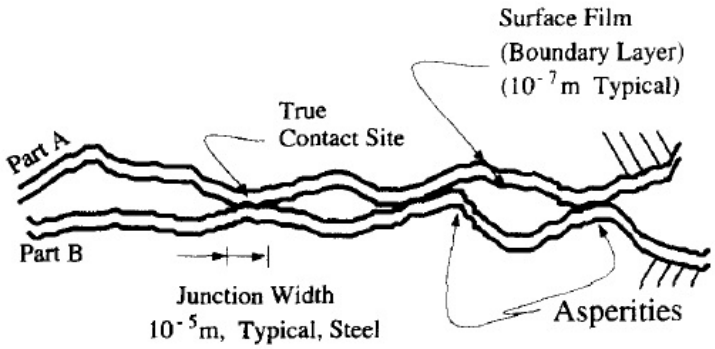

Figure 2.5: Presliding regime [2].

(ii) Boundary lubrication regime: In this regime, fluid film is not formed because of the low velocity and in some parts lubrication occurs (Figure 2.6).

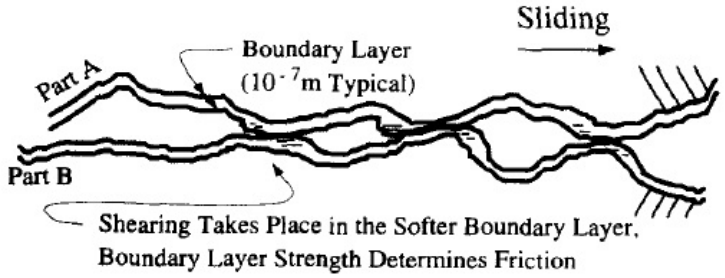

Figure 2.6: Boundary lubrication [2].

(iii) Partial fluid lubrication regime: Higher velocity causes thicker fluid film. If the asperity's height is thicker than film, there will be partial fluid lubrication. While partial fluid lubrication increases, solid-solid contact and friction reduces (Figure 2.7).

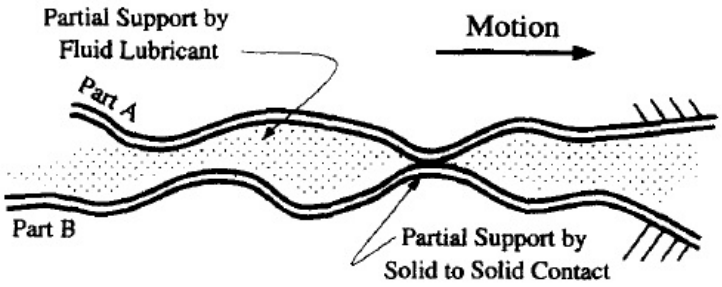

Figure 2.7: Partial fluid lubrication [2].

iv) Full fluid lubrication or sliding regime: There is no solid-solid contact and sliding occurs (Figure 2.8).

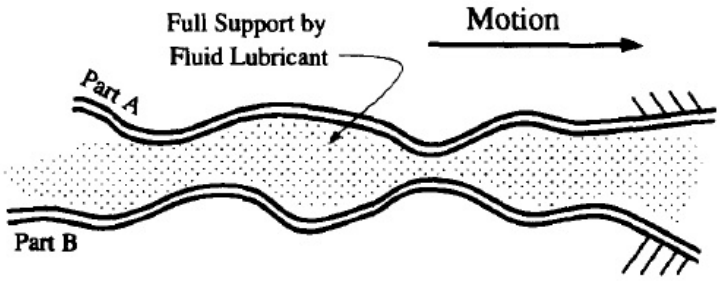

Figure 2.8: Full fluid lubrication [2].

As mentioned, there are different friction behaviors in different regimes, changing from pre sliding to sliding regimes. In order show these changes, friction can be modeled in various forms such as algebraic equations or hybrid models [3]. Complete friction modeling by describing all the physical and material/surface properties has not been achieved yet. There exist research works focused on developing physically motivated models with sufficient friction identification and compensation based on experimental data [15].

There are different kinds of friction models described in the literature. The survey of Armstrong et. al. is the first atttempt to unify different friction models in one study [2]. In this survey, the author gives some classical (static) friction model descriptions and dynamical models. In general, friction force is a function of velocity and the applied force for static friction models. On the other hand, for the dynamic friction models, friction

force is a function of displacement. In this section, some of the friction models will be explained.

2.1.2.1 Classical (Static) Friction Models

This type of friction is generally written as a combination of Coulomb, viscous, static and Stribeck frictions. General name of this type of friction is called classical or static friction models in the literature. As can be seen from Figure 2.9, each type of friction feature has different characteristic while velocity changes. Figure 2.9.b shows the characteristic of viscous friction plus Coulomb friction. Figure 2.9.c shows the Stribeck effect: During the boundary lubrication, friction force decreases while velocity increases and then friction force starts increasing as velocity gets larger. In this type of friction model, during pre sliding regime, there is no specified friction force around zero velocity. This is the main drawback of the static friction model. In addition, different forms of classical models are used in the literature [3], [7], [8].

Simple friction force that is combination of viscous and Coulomb friction forces can be formulated as [11]

$$F_f = \begin{cases} F_C^+ + F_v v & v \geq 0, \\ F_C^- + F_v v & v < 0. \end{cases} \tag{2.3}$$

Here, F_C^+, F_C^- represent the Coulomb friction forces and F_v is viscous friction term. v is the velocity.

General formulation of static friction proposed by Amstrong et. al. is [2]:

$$F_f = \begin{cases} F(v) & \text{if } v \neq 0 \\ F_e & \text{if } v = 0 \text{ and } |F_e| < F_S \\ F_S sgn(F_e) & \text{if } v = 0 \text{ and } |F_e| \geq F_S \end{cases} \tag{2.4}$$

$$F(v) = F_C + (F_S - F_C)e^{-|v/v_S|^{\delta_S}} + F_v v \tag{2.5}$$

Here, $F(v)$ is an arbitrary function and identification of $F(v)$ can be done by measuring the friction force for different constant velocities [3]. F_e is an external force applied to the system and F_S is the static force. In addition, v_S is the Stribeck velocity and δ_S is the shape factor for Stribeck velocity. Another model that is presented in [3] is the following

$$F_f = \begin{cases} F_S^+ e^{-v/v_{S1}^+} + F_C^+(1 - e^{-v/v_{S2}^+}) + F_v v & v \geq 0 \\ F_S^- e^{-v/v_{S1}^-} + F_C^-(1 - e^{-v/v_{S2}^-}) + F_v v & v < 0 \end{cases} \tag{2.6}$$

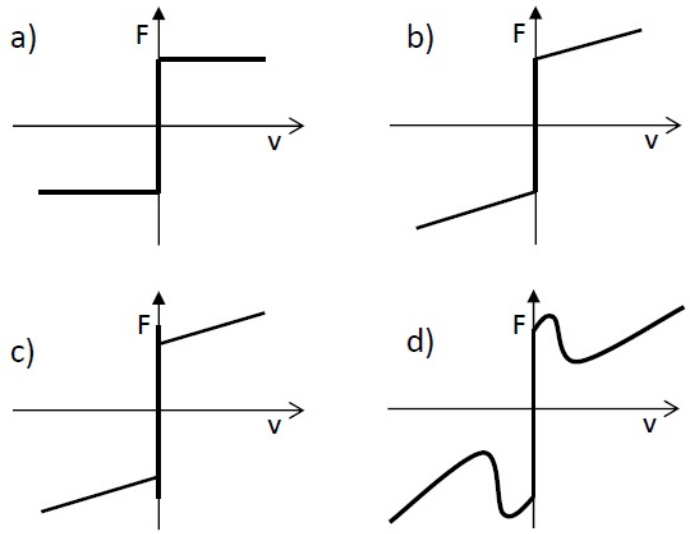

Figure 2.9: Examples of static friction models. a)Coulomb friction, b)Coulomb+viscous friction, c)Static+Coulomb+viscous, d)Static+Coulomb+viscous+stribeck friction.

Here, v_{S1}^{+}, v_{S1}^{-}, v_{S2}^{+} and v_{S2}^{+} represent the velocity constants that determine velocity spacing between different friction regions. Value of these terms depend on viscosity and temperature of the working place.

However, as mentioned, detecting friction force around zero velocity is still a challenge. There has been several studies to overcome this problem. Karnopp proposed a model that tries to handle this drawback and simulates another nonlinear friction phenomenon, namely stick-slip friction [16]. Stick slip is a jerky motion that occurs during high sliding velocity for small friction force. For example, wipers of the cars, when the window glass is partially wet, go through a stick slip motion. This friction feature is not desirable for precise machine tools [7]. In order to model this effect and handle the friction force problem around zero velocity, Karnopp defined zero velocity tolerance $|v| < \epsilon$ for some small $\epsilon > 0$. In this region, friction force is defined as a function of other forces in the system as opposed to function of velocity for sliding regime. A disadvantage of Karnopp model is that the external force is not exact and the model is strongly coupled with the rest of the system [7].

2.1.2.2 Dynamic Models

Various dynamic friction models were proposed in the literature, aiming to enhance the static ones. Some widely used ones of these models will be presented below.

The Dahl Model

This model was proposed for dynamical system for both rolling and sliding friction simulations. The Dahl model only relates with pre sliding regime. During experimentation of ball bearings behavior, the author first observes that as a result of small displacements in the rest position, an elastic restoring force arises on the balls. Then, he focuses on strength features of solid materials and concludes that bearing and solid frictions behave similarly. While examining stress-strain curve of solid materials, he sees that stress-strain characteristic can be used for friction force-displacement relationship. He then proposes basic equations for this relationship in [17]. This model's mathematical equations were further discussed in [18]. The general formulation is given as

$$\frac{\mathrm{d}F_f}{\mathrm{d}x} = \sigma \left| 1 - \frac{F_f}{F_C} sgn(v) \right|^i sgn\left(1 - \frac{F_f}{F_C} sgn(v) \right), \tag{2.7}$$

where σ is the initial stiffness at velocity reversal, F_C is the Coulomb friction force, which equals to static friction force, v is velocity, and i is the model exponent parameter that defines hysteresis shape.

The Dahl model also represents rate independence property, which means that the speed of the input values (in this case input is displacement) between extremum points do not affect the branching. In other words, time effects between two extremum points are negligible [19]. This feature has an important role in the use of the theory of the hysteresis operators [9], [20]. In addition, this model is an important study for describing the position dependent hysteresis loops. Yet, it does not include Stribeck effect and break away force [7]. This model is further discussed and used by other researchers in original and modified forms [21], [22], [23].

The LuGre Model

Since Dahl friction model does not cover Stribeck effect, there has been several studies to overcome this problem. One of them is the LuGre model, a dynamic friction model, incorporating the static friction features with Stribeck effect [4]. In this model, the idea is to represent surface contact by fictitious bristles in the macroscopic level, as demonstrated in Figure 2.10.

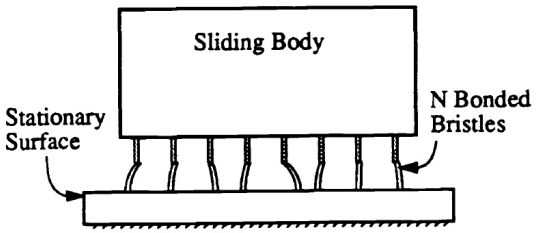

Figure 2.10: The bristle model [34].

The LuGre model mainly focuses on the fictitious bristles and considers average deflection z of these bristles. The time derivative of this average deflection is modeled as

$$\frac{\mathrm{d}z}{\mathrm{d}t} = v - \frac{|v|}{g(v)}z, \tag{2.8}$$

where v is the velocity of the sliding surface and $g(v)$ represents the Stribeck friction, i.e.,

$$\sigma_0 g(v) = F_C + (F_S - F_C)e^{-|v/v_S|^2} \tag{2.9}$$

where σ_0 is the stiffness coefficient and the velocity constant v_S determines the velocity spacing between different friction regions. F_S and F_C is coulomb and static friction, respectively.

The friction force is given by

$$F_f = \sigma_0 z + \sigma_1 \frac{\mathrm{d}z}{\mathrm{d}t} \tag{2.10}$$

where σ_1 is the viscous damping coefficient. Including viscous friction, (2.10) becomes

$$F_f = \sigma_0 z + \sigma_1 \frac{\mathrm{d}z}{\mathrm{d}t} + \sigma_2 v, \tag{2.11}$$

where σ_2 is the viscous friction coefficient.

Although LuGre model includes friction phenomena such as friction lag, break away force, etc., the model does not include hysteresis effects with nonlocal memory. In the hysteresis with nonlocal memory, the future friction force values do not only depend on the present values of displacement or friction force but depend on past extremum values

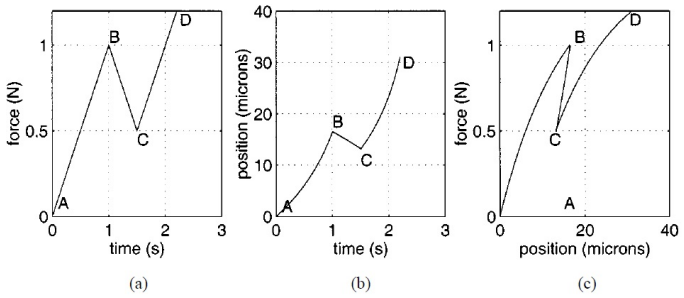

Figure 2.11: Lugre model simulation results [5].

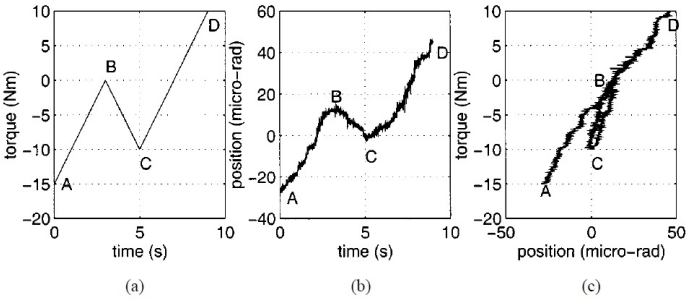

Figure 2.12: Experimental results of Lugre model [5].

of friction force as well [19]. Furthermore, Swevers states that the LuGre model has a deficiency due to the fact that it is not capable of attune itself for arbitrary force-displacement transition curves. Typical simulation and experimental results of the LuGre model are shown in Figures 2.11 and 2.12.

The Leuven Model

As mentioned above, the main drawback for LuGre model is not capturing hysteresis with nonlocal memory. Swevers developed the Leuven model to deal with this problem and included various friction features in one formulation [5]. There are two main equations for the friction force, which depend on the state z-the average deflection of the bristles:

$$F_f = F_h(z) + \sigma_1 \frac{dz}{dt} + \sigma_2 v, \tag{2.12}$$

$$\frac{dz}{dt} = \left(1 - sgn\left(\frac{F_d}{s(v) - F_b}\right)\left|\frac{F_d}{s(v) - F_b}\right|^n\right), \tag{2.13}$$

where $F_h(z) = F_b + F_d(z)$ represents the hysteresis friction force, σ_1 and σ_2 are micro-viscous damping and the viscous friction coefficients. Current transition curve friction force is given by F_d, and F_b represents the friction force at the beginning of the transition curve. Stribeck velocity term is represented by $s(v)$.

Lampaert et. al. is made some modifications to the Leuven model in [24]. Firstly, there occurs a problem because F_b equals to the former value of $F_h(z)$ in each transition cycle. Therefore, this does not make any change in the equation $F_h(z) = F_b + F_d(z)$. This problem is handled by replacing $F_d(z)/(s(v) - F_b)$ with $F_h(z)/s(v)$ and (2.13) becomes

$$\frac{dz}{dt} = \left(1 - sgn\left(\frac{F_d}{s(v) - F_b}\right)\left|\frac{F_h(z)}{s(v)}\right|^n\right) \tag{2.14}$$

In a couple of velocity reversals, there occurs more than one hysteresis loops, each of them called stack. The Leuven model does not take stack size into consideration. Second modification was made by choosing stack size in advance to prevent stack overflow. Lampaert et. al. proposed the following Maxwell slip model for the hysteresis force.

Generalized Maxwell Slip (GMS) Model

The so called generalized Maxwell slip model was proposed in [6]. This friction model includes three main friction phenomena namely, the hysteresis with nonlocal memory, the Stribeck curve for constant velocities, and the frictional lag. Figure 2.13 demonstrates the general Maxwell slip model with N elementary units. There is one common input z for both stick and slip regimes. The model is based on two main equations for sliding and pre sliding regimes.

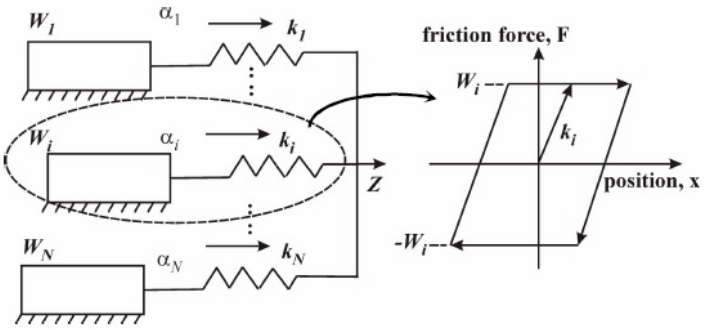

Figure 2.13: Maxwell slip model [8].

For each unit, when the unit is sticking, the state equation is

$$\frac{dF_i}{dt} = k_i v. \tag{2.15}$$

Sticking continues until F_i reaches $W_i = \alpha_i s(v)$, where F_i is the friction output, W_i is the maximum elementary Coulomb force, α_i and k_i represent the normalized sustainable maximum friction force of each unit during sticking and an elementary stiffness, respectively. When the element is slipping, the state equation is given by

$$\frac{dF_i}{dt} = sign(v)C\left(\alpha_i - \frac{F_i}{s(v)}\right) \tag{2.16}$$

where $s(v)$ is a Stribeck function.

$$s(v) = sgn(v)(F_C + (F_S - F_C)e^{-|v/v_S|^\delta})$$

where F_S and F_C are static and Coulomb friction forces. v_S is the velocity constant. C is the constant parameter which represents the rate at which the friction force follows the Stribeck effect in sliding. The overall friction force is proposed as the summation of the outputs of all elementary state models plus viscous term σ.

$$F_f(v) = \sum_{i=1}^{N} F_i(v) + \sigma v(t) \tag{2.17}$$

2.2 Offline System Identification and Feedforward Compensation Design

2.2.1 System Identification of Multi Axis Dynamics

For feed drive systems, identification of axis dynamics and decreasing some positioning errors with optimal performance have attracted a lot of researchers. In order to accomplish desired performance before examining friction identification, feed drive system parameters like inertia and viscous damping coefficients need to be identified because inaccurate identification of these parameters cause problem in the rest of controller design.

Different kinds of parameter identification techniques are discussed in the literature [8], [3]. Erkorkmaz [3] used simple least square algorithm to capture feed drive parameters. In this procedure, piecewise constant current commands are used to excite the system. In addition, the reference signal is selected such that it originates large signal for high acceleration and long signal for high velocities in order to identify inertia and viscous damping parameters properly. It should be noted that the author uses simple friction model for identification purposes; F_C^+ for $v > 0$ and F_C^- for $v < 0$. Because of the Coulomb friction's amplitude dependency, the pulse's amplitude is also selected to vary in time [3], [12]. One other approach is to collect frequency domain measurements from the system of interest and fit the tuned inertia and viscous friction parameters to match with the measurements [8], [13].

2.2.2 Offline compensation of friction

In the literature, different friction compensation techniques have been proposed. Some of the compensation methods used in the literature are classical PD, PID controllers, dither, impusive, and joint torque control etc. [7]. In the following paragraph, mainly used mainly used compensation techniques are discussed.

The general block diagram for feedforward friction compensation technique is given in the Figure 2.14. In order to conduct feedforward compensation approach accurately, friction model parameters needs to be as close as possible to their actual values. Offline friction parameter identification techniques were used in the literature for designing friction model parameters realistically. Kalman filter [25] and inverse-model based observers [8], for example, are used to obtain friction force by using disturbance observation. The friction parameters are designed according to disturbance observation by considering the friction

as the only source of disturbance in the system. After this procedure, parameters identified using disturbance observation is used in feed-forward compensator process.

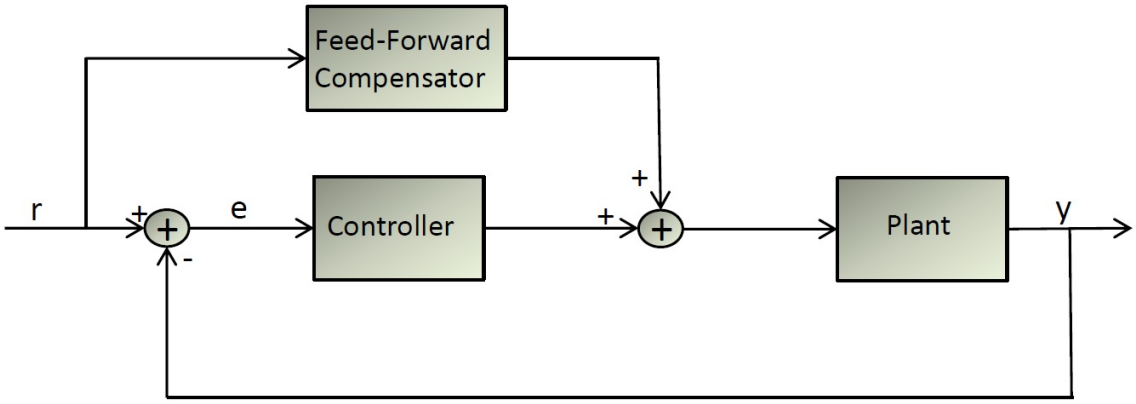

Figure 2.14: General ball-screw drive motion control scheme with feedforward friction compensation.

2.3 Online Parameter Estimation and Adaptive Feedback Control Design

Online parameter estimation is the second way of performing friction compensation. Generally, as in the Section 2.2, the friction models are nonlinear. Thus, this makes adaptive compensation challenging. In order to use robust identification techniques like recursive least square algorithm or adaptive model reference control, system needs to be either simplified in parameters or partially known.

In practical cases for adaptive control, the system is generally assumed to be partially known that is because of ease of online estimation design. Canudas and Astrom [11] use DC motor with permanent magnet for experimental purpose. The authors use the simple classical model that includes viscous and Coulomb friction features and defines friction force equation as

$$F_f = sgn(w)(F_c + F_v w) \tag{2.18}$$

Here w is the angular velocity of the DC motor. F_v avd F_c are viscous and coulomb friction, respectively. Recursive least square algorithm is used to estimate the parameters of

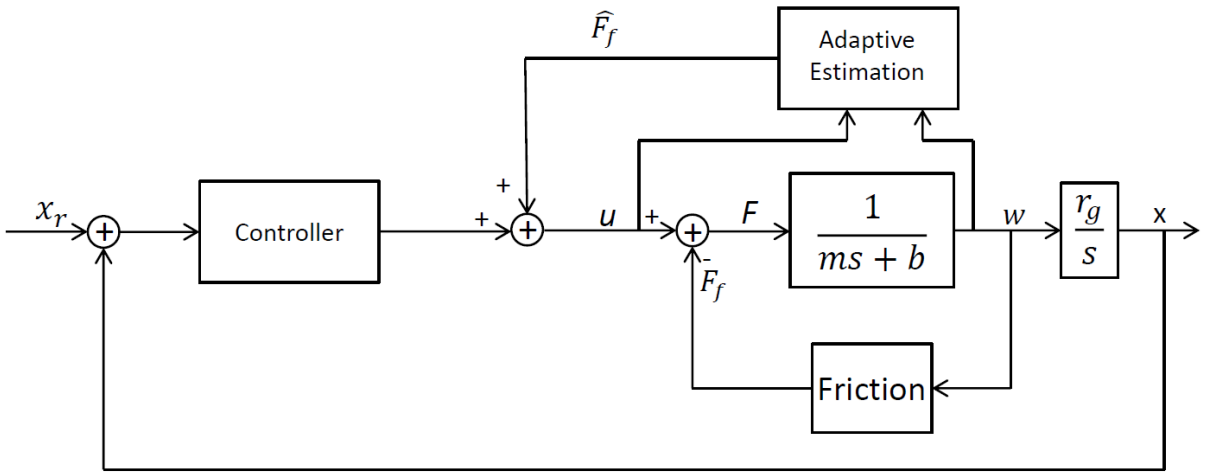

Figure 2.15: General adaptive motion control scheme, with online friction estimation and compensation.

friction model below (Figure 2.15). In the experimental analysis of the model, they compare offline and online methods. As expected, adaptive compensation gives less tracking error than offline methods.

Using classical friction model, adaptive control technique is also used for robotic manipulator during for velocities [26]. The author overcomes stability issues caused by adaptive controller to modify overall system transfer function and add a dither noise to the input torque. In order to estimate unknown parameters, he uses a weighted least square algorithm. Results are considerable during adaptive estimation, but still more realistic model needs to be used. Furthermore, for different systems, some of the other adaptive laws used to identify static friction model parameters [10], [27].

Chapter 3

A New Least-Squares Based Adaptive Control Scheme

Online parameter identification (PI) algorithms process the past and current measurements of signals and generate an estimate of unknown plant parameters at each time. There is a wide range of adaptive laws for online PI with different convergence features [28]. In this chapter, we propose a least-squares based adaptive law for common static friction models for ball screw drive system, and then develop an adaptive motion control scheme based on this adaptive law.

3.1 Least-Squares Based On-Line Identification

There are in general three main steps to build on-line PI algorithms; forming a parametric model (PM), designing an adaptive algorithm, and establishing conditions to guarantee that the parameter estimates converge to their actual values. For the PM construction step, we consider two types of generic static friction models are given in equations (2.3) and (2.6) and the following equations will be constructed according to these types of static friction models. Taking into account steps that given above, the least square algorithm can be designed.

Consider the plant model

$$(m/r_g)\ddot{y} + (b/r_g)\dot{y} = F = u - F_f$$

where m is the mass and b is the viscous friction coefficients for rigid body motion. r_g is the rotation to linear conversion factor. y and $\dot{y}$ are linear displacement and velocity,

respectively. $w = \dot{y}/r_g$ refers to angular velocity. F_f represents the friction force and F is the net force that is applied to the plant.

Transfer function of the plant from F to y is

$$G_p(s) = \frac{r_g}{s}\frac{1}{ms+b}$$

Mass and viscous friction coefficients (m,b) are assumed to be precisely obtained via an off-line identification process, example of which is given in Chapter 4. It should be noted that because of the air bearings, viscous daming is very small and is not taken into account. In addition, y and w are measurable signals.

3.1.1 Static Friction Model 1

We first construct an online PI algorithm based on Equation (2.3).

Step 1.Parametric model:
y and w are known signals, we can express (2.3) in the static PM (SPM) form.

$$z_w = \theta^{*T}\phi_w, \tag{3.1}$$

Here, z_w and ϕ_w are available for measurements.

$$z_w = \frac{1}{\Lambda(s)}[u] - \frac{ms+b}{\Lambda(s)}[w] \tag{3.2}$$

In order to avoid differentiation, the signals can be filtered with a stable filter of relative degree one, e.g., $1/\Lambda(s)$ with $\Lambda(s) = s+\lambda = s+5$, which is a stable polynomial. Unknown parameters can be expressed as

$$\theta^* = [F_C^-, F_C^+, F_V]^T$$

F_C^-,F_C^+ are Coulomb friction parameters that need to be identified for negative and positive directions of motion. F_V, viscous friction term, is opposite to the direction of motion.

$$\phi_w = \frac{1}{\Lambda(s)}[\sigma^-(w), \sigma^+(w), \sigma^o(w)w]^T$$

In order to avoid the direction misinterpretations, threshold term $\psi = 0.01$ is used. In the case of $\psi = 0$, estimation slows down or gives unbounded results.

$$\sigma^o(w) = \begin{cases} 1 & |w| \geq \psi \\ 0 & |w| < \psi \end{cases}$$

$$\sigma^-(w) = \begin{cases} 1 & w < -\psi \\ 0 & w \geq -\psi \end{cases}$$

$$\sigma^+(w) = \begin{cases} 0 & w < \psi \\ 1 & w \geq \psi \end{cases}$$

Step 2.Parameter Identification Algorithm

Estimation Model

$$\hat{z}_w = \theta^T \phi_w \tag{3.3}$$

where $\theta(t)$ is the estimate of θ^* at time t.

Estimation Error:

$$\varepsilon_w = z_w - \hat{z}_w = z_w - \theta^T \phi_w \tag{3.4}$$

According to below adaptive law, at each time t, $\theta(t)$ adjusts it self and ε gets smaller and smaller through the time. Afterwards, the unknown parameters converge their actual values.

Adaptive Law:

Using recursive least square algorithm with forgetting factor,

$$\begin{aligned} \dot{\theta} &= P\varepsilon_w \phi_w, & \theta(0) &= \theta_0 \\ \dot{P} &= \beta P - P\phi_w \phi_w^T P, & P(0) &= P_0 \end{aligned} \tag{3.5}$$

Here, P is the covariance matrix and β is the forgetting factor.

Step 3.Stability and Parameter Convergence

If ϕ is persistently exciting (PE), the recursive least square algorithm with forgetting factor (3.4) guarantees that $P, P^{-1} \in \mathcal{L}_\infty$ and that $\theta(t) \to \theta^*$ as $t \to \infty$. The convergence of $\theta(t) \to \theta^*$ is exponentially when $\beta > 0$ [28]. Despite of the fact that ϕ needs to be PE for convergence condition, it should be noted that this condition might not hold for all systems. Therefore, parameters may converge to their actual value without PE condition.

3.1.2 Static Friction Model 2

In the Equation (2.6), Stribeck velocity constants are assumed to be known parameters. Real values of these constants are taken from [3]. The other unknown friction model parameters are given in the following equations. For the estimation purpose, the actual values of these parameters in [3] are used. The purpose is to generate online estimates for friction force parameters.

Step 1.Parametric model:

Since y and w are known signals, we can express SPM [28] as

$$z_w = \theta^{*T}\phi_w,$$

Here, z_w and ϕ_w are available for measurements.

$$z_w = \frac{1}{\Lambda(s)}[u] - \frac{ms+b}{\Lambda(s)}[w]$$

In order to avoid differentiation, the signals can be filtered with a stable filter of relative degree one, e.g., $1/\Lambda(s)$ with $\Lambda(s) = s + \lambda = s + 5$, which is a stable polynomial.

$$\theta^* = [F_S^-, F_C^-, F_S^+, F_C^+, F_V]^T$$

F_S^-,F_C^- are static and Coulomb friction parameters that need to be identified for negative direction of motion. On the other hand, F_S^+,F_C^+ are parameters for positive direction of motion. F_V, viscous friction term, is opposite to the direction of motion. Since this term is assumed to be inversely proportional to the velocity in the equation, it can be identical for both direction.

$$\phi_w = \frac{1}{\Lambda(s)}[g^-(w)f_1^-(w), g^-(w)f_2^-(w), g^+(w)f_1^+(w), g^+(w)f_2^+(w), g^o(w)w]^T$$

Here,

$$f_1^+(w) = e^{-w/v_{S1}^+}$$
$$f_2^+(w) = 1 - e^{-w/v_{S2}^+}$$
$$f_1^-(w) = e^{-w/v_{S1}^-}$$
$$f_2^-(w) = 1 - e^{-w/v_{S2}^-}$$

v_{S1} and v_{S2} can take different values for different systems. This term is assumed to be available. Therefore, above functions become known parameters for different directions. In addition, in order to avoid the direction misinterpretations, threshold term $\psi = 0.01$ is used. In the case of $\psi = 0$, estimation slows down or gives different results.

$$g^o(w) = \begin{cases} 1 & |w| \geq \psi \\ 0 & |w| < \psi \end{cases}$$

$$g^-(w) = \begin{cases} 1 & w < -\psi \\ 0 & w \geq -\psi \end{cases}$$

$$g^+(w) = \begin{cases} 0 & w < \psi \\ 1 & w \geq \psi \end{cases}$$

Here, according to velocity value, unknown parameters converge either their actual values.

Step 2.Parameter Identification Algorithm

Parameter identification algorithms are also going to be the same as equations (3.3), (3.4) and (3.5).

Step 3.Stability and Parameter Convergence

In order to guarantee convergence, ϕ needs to be PE. Conditions that are given above also holds for this type of friction model.

3.2 The Adaptive Control Scheme

In this section friction estimation results are given. The general adaptive control scheme is given in Figure 3.1. By giving net force (F) and rotary feedback signal (w), estimation of friction force ($\hat{F}_f$) is identified. Since the friction force is opposite to the direction of motion, estimated friction force is added to the closed loop system.

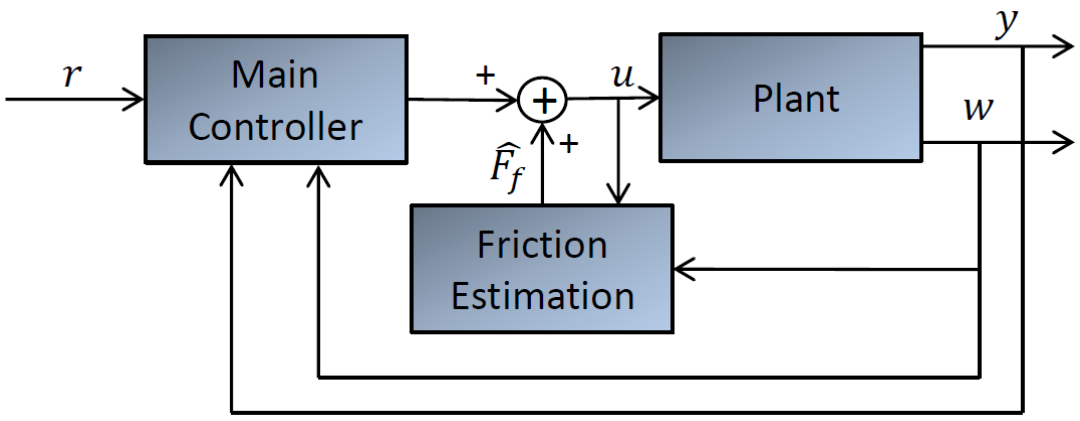

Figure 3.1: Adaptive control scheme.

3.2.1 Nominal Controller

In industrial automation, various servo controllers ranging from simple PID to more complex loop structures are used. The purpose of using servo controllers is to stabilize the motion and end-effectors to have to track reference positions accurately, i.e., have the tracking errors at tolerably small levels. In this study, two types of controllers are designed to be incorporated with the PI algorithms presented in Section 3.1. Firstly, a backstepping controller is proposed in order to show adaptive identification effect in perfect tracking condition. Secondly, a more classical P-PI controller is designed for two types of classical friction models.

3.2.1.1 Backstepping Controller

We rewrite the system equations in state-space form as

$$\dot{x_1} = r_g x_2, \tag{3.6}$$
$$\dot{x_2} = (-b/m)x_2 + (r_g/m)u, \tag{3.7}$$
$$x_1 = y, \qquad x_2 = w$$

We want to design a controller that helps the output signal $x_1 = y$ to follow reference signal r, i.e. it is desired to satisfy $e_1 = x_1 - r \to 0$ asymptotically. This would be satisfied if we have the dynamics

$$\dot{e}_1 = -Ke_1$$

where $K > 0$ is some feedback constant. To investigate further, rewrite (3.6) as

$$\dot{e}_1 = -Ke_1 + e_2 \tag{3.8}$$

where

$$e_2 = \dot{e}_1 + Ke_1 = \dot{x}_1 - \dot{r} + Ke_1 = r_g x_2 - \dot{r} + Ke_1 \tag{3.9}$$

It is also desired to have e_2 diminishing asymptotically. The dynamic for e_2 is derived from (3.7)-(3.9) as

$$\dot{e}_2 = K\dot{e}_1 + r_g\dot{x}_2 - \ddot{r} = -K^2e_1 + Ke_2 - \ddot{r} - (br_g/m)x_2 + (r_g/m)u \tag{3.10}$$

Denoting,

$$v = -\ddot{r} - (br_g/m)x_2 + (rg/m)u, \tag{3.11}$$

the derivative of e_2 becomes

$$\dot{e}_2 = -K^2e_1 + Ke_2 + v. \tag{3.12}$$

Consider the Lyapunov function

$$V = \frac{1}{2}(e_1^2 + \gamma e_2^2) \tag{3.13}$$

where $\gamma > 0$. Taking derivative of Lyapunov function, we obtain,

$$\dot{V} = e_1\dot{e}_1 + \gamma e_2\dot{e}_2$$

Subtracting $\dot{e}_1$ and $\dot{e}_2$ with equations (3.6)-(3.8), we get,

$$\dot{V} = -Ke_1^2 + e_1e_2 - \gamma K^2e_1e_2 + \gamma Ke_2^2 + \gamma e_2v \tag{3.14}$$

Let $\gamma = \frac{1}{K^2}$. Then,

$$\dot{V} = -Ke_1^2 + \frac{1}{K}e_2^2 + \frac{1}{K^2}e_2v$$

Choosing

$$v = -2Ke_2 \tag{3.15}$$

yields

$$\dot{V} = -Ke_1^2 - \frac{1}{K}e_2^2 \tag{3.16}$$

which implies asymptotic stability for all $K > 0$. Hence, to obtain (3.16), we choose the control signal based on (3.11) and (3.15) as

$$\begin{aligned} u &= \frac{-2Km}{r_g}e_2 + \frac{b}{r_g}x_2 + \frac{m}{r_g}\ddot{r} \\ &= -2Km(x_2 - \frac{\dot{r}}{r_g} + K(x_1 - r)) + \frac{b}{r_g}x_2 + \frac{m}{r_g}\ddot{r} \\ &= (-2K^2m)x_1 + (-2Km + \frac{b}{r_g})x_2 + (2K^2m)r + \frac{2Km}{r_g}\dot{r} + \frac{m}{r_g}\ddot{r} \end{aligned}$$

In our later implementation work, we have chosen $K = 1$ for simplicity.

3.2.1.2 P-PI Controller

The general representation of P-PI controller is given in Figure 3.3. The general idea for this type of controller is to put velocity loop inside the position loop. Two generated signals are used for controller inputs; namely angular velocity and linear displacement signals. Friction and some modeling errors can cause positioning errors during motion of machine tools. Especially, during change of motion direction, such errors might cause direction misinterpretation and instability issues. In order to overcome this problem, speed feedforward term is used. In other words, this term is added up to velocity loop to ensure that feedback controller follows reference signal properly. Table 3.1 represents gains that are used for P-PI controller.

Control signal equivalent mass	m [V/(rad/s^2)]	0.0022
Conversion factor	r_g [mm/rad]	3.1831
Position controller gain	K_{p1} [(rad/s)/mm]	240
Velocity controller gain	K_{p2}[V/(rad/s)]	0.8
Integral gain	K_i[V/rad]	25

Table 3.1: Parameters for simulation.

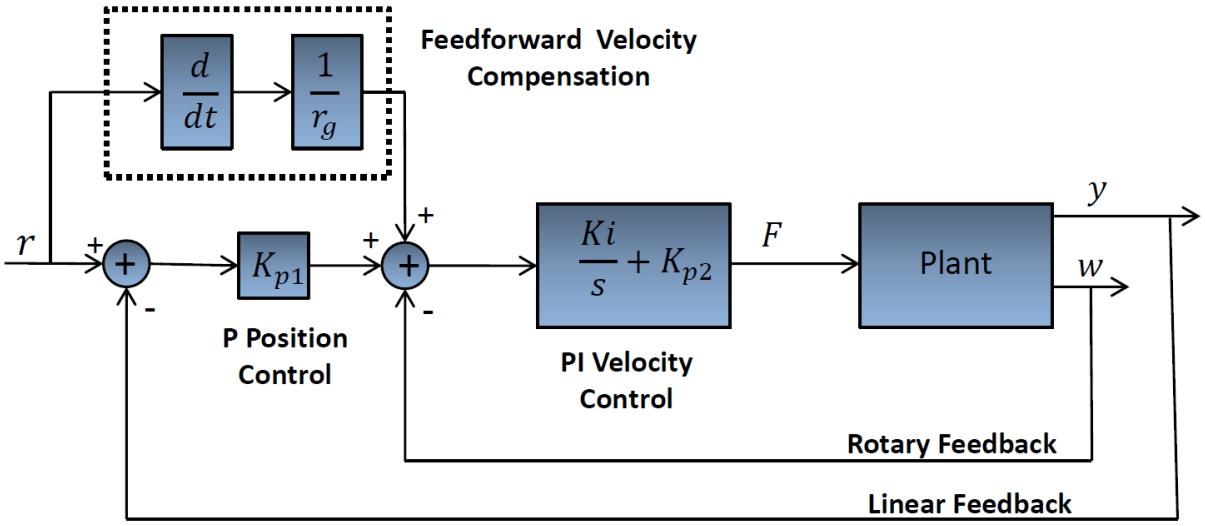

Figure 3.2: P-PI controller scheme

3.3 Simulations and Experiments

This section presents the results of simulation and experimental testing of the adaptive control with feedback controllers. In the first part, backstepping controller simulation results are discussed. Afterwards, P-PI controller analysis is explained for two types of friction models given in the equations (2.3) and (2.6). In addition, off-line experimental results will be given for static friction model 2.

3.3.1 Adaptive Backstepping Control Scheme

Backstepping simulation results are given in Figure 3.3 and 3.4. Simulations are repeated for two different scenarios; firstly, when the plant is affected by friction force and adaptive estimation algorithms are disabled. Secondly, the adaptive control is activated and on-line compensation affects are examined.

When the friction is added to the feed drive dynamics, friction affect leads to 2 mm tracking error (Figure 3.3.b). In addition, in the Figure 3.4, adaptive control results can be seen. There is over 1.8 mm tracking error for 2 seconds. After 2 seconds, these errors decrease through time and reach around zero.

As it is demonstrated in the Figure 3.5, friction parameters converge their actual values

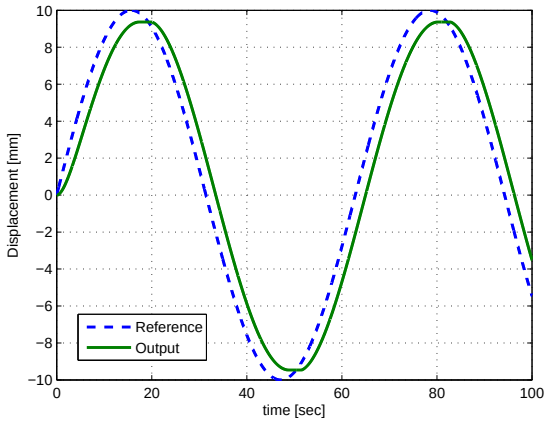

(a) Reference vs output signals.

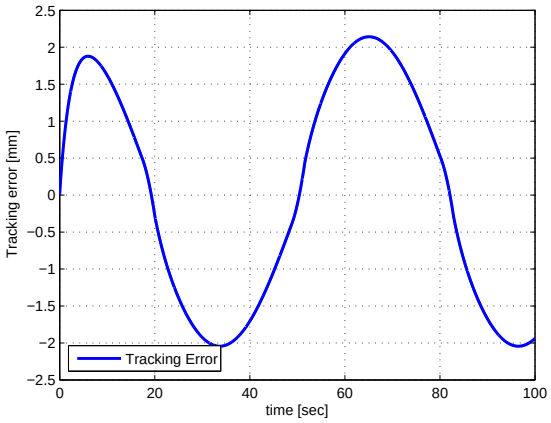

(b) Tracking error.

Figure 3.3: Non-adaptive backstepping control of the ball-screw drive system without friction compensation.

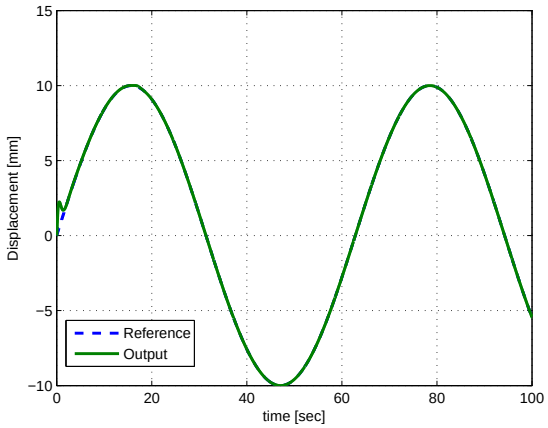

(a) Reference vs output signals.

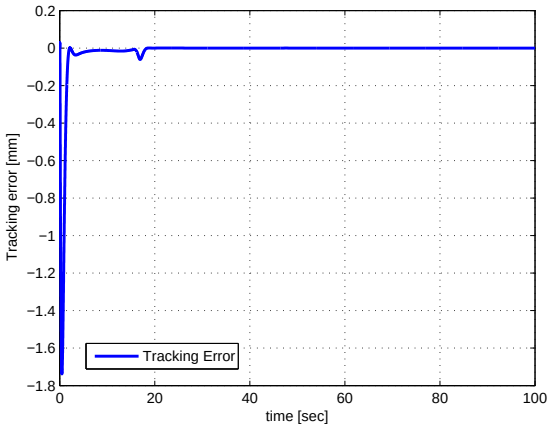

(b) Tracking error.

Figure 3.4: Adaptive backstepping control of the ball-screw drive system with friction compensation.

after 48 seconds. Since friction changes with velocity, friction versus velocity graph is also constructed (Figure 3.6). From this graph, it can be seen that convergence is successful.

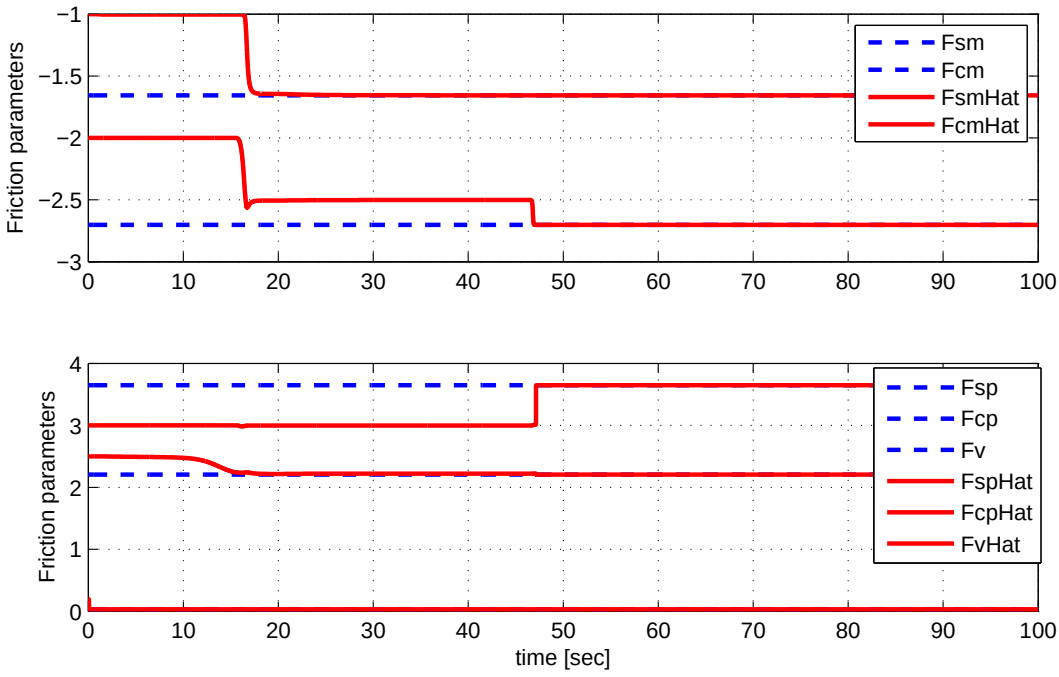

Figure 3.5: Parameter estimation results for adaptive backstepping control scheme.

3.3.2 Adaptive P-PI Control Scheme

In this section, firstly, friction model that's adaptive control law is given in the Section 3.1.1 will be used in the simulations with P-PI controller. Afterwards, simulation and experimental results for the friction model that is given in Equation 2.6 is going to be explained.

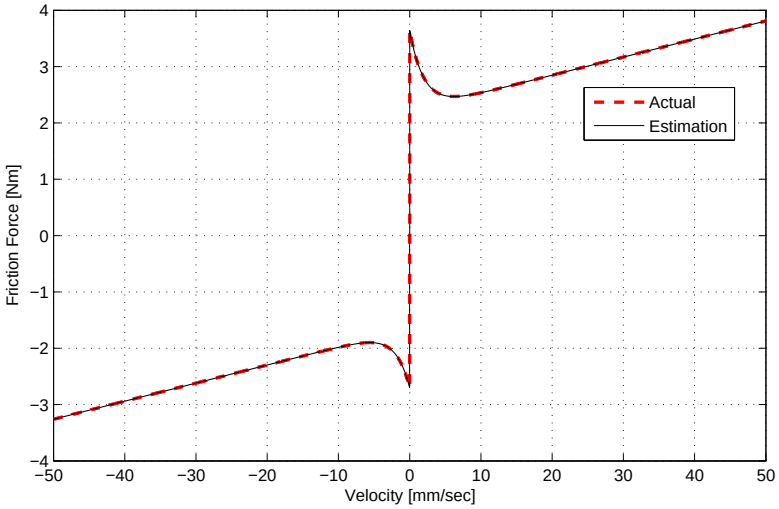

Figure 3.6: On-line identification results at the end of adaptive backstepping control run.

3.3.2.1 Static Friction Model-1

Simulation Results:

Figure 3.7 and 3.8 shows the reference and output signal results. As it is shown, there is 0.003 mm tracking error when there is feedback controller and friction applied to the dynamics (Figure 3.7.b). On the other hand, when adaptive control is enabled, tracking error goes to zero after 30 seconds (Figure 3.8.b). Convergence results are given in the Figure 3.9.

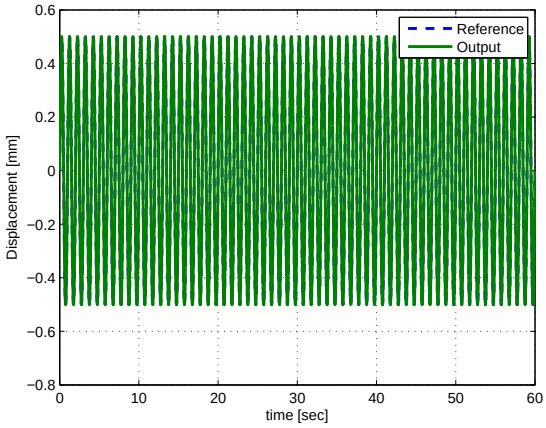

(a) Reference vs output signals.

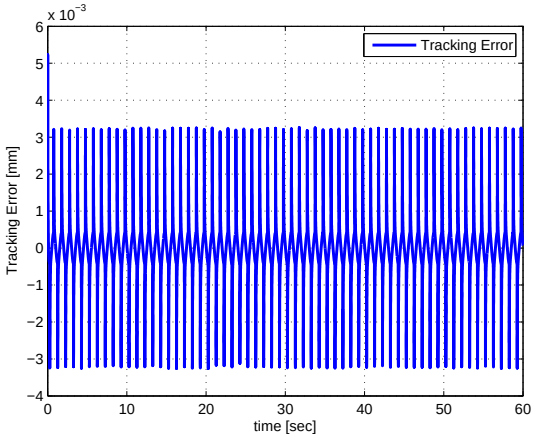

(b) Tracking error.

Figure 3.7: Non-adaptive PPI control results with static friction model 1.

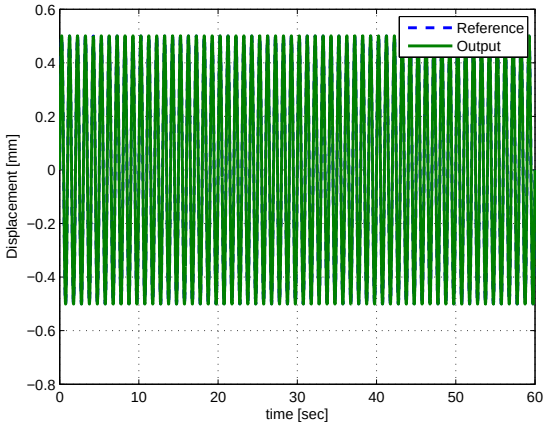

(a) Reference vs output signals.

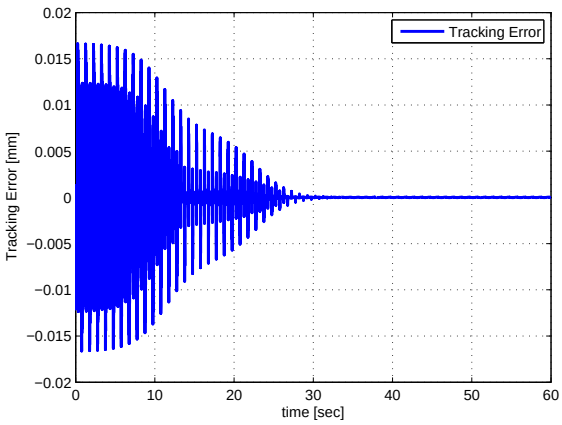

(b) Tracking error.

Figure 3.8: Adaptive PPI control scheme results with static friction model 1

Experimental Results:

Control signal, rotary feedback signal, and output signals are collected from ball screw drive setup. Rotary feed back signal (angular velocity) and control signals are given estimation block as input signals. Reference vs ouput signals and tracking error that obtained

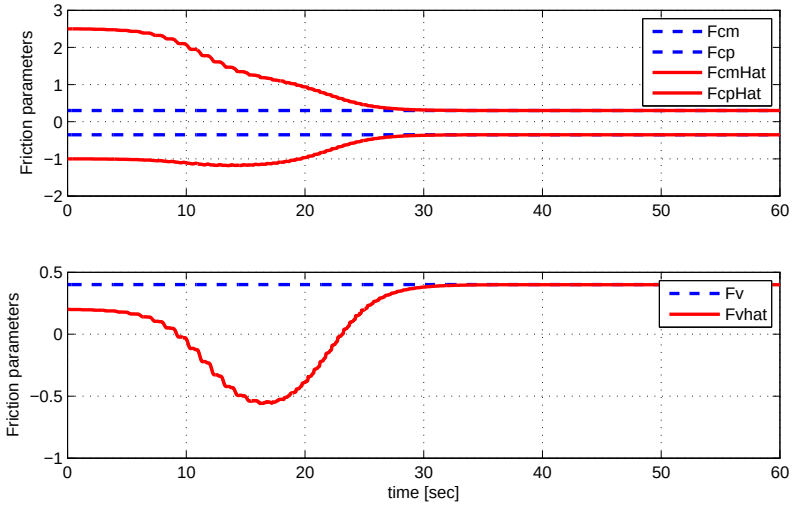

Figure 3.9: Parameter estimation results for adaptive PPI control scheme with static friction model 1.

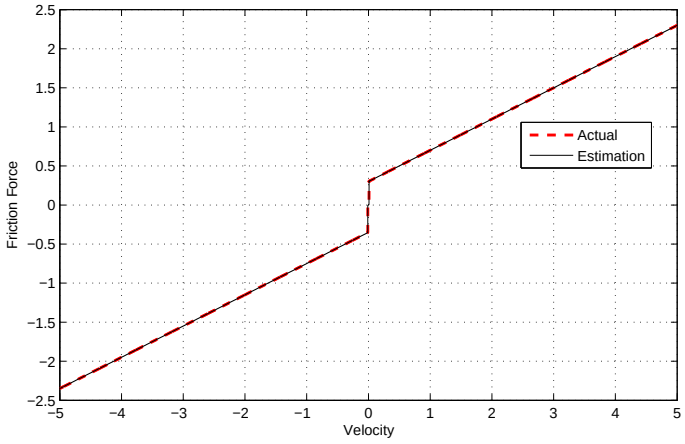

Figure 3.10: On-line parameter identification results at the end of adaptive PPI control run with static friction model 1.

from experimental setup given in Figure 3.11. During adaptive compensation, for static friction model 1, it is observed that affects of friction is eliminated after 30 seconds (Figure 3.12).

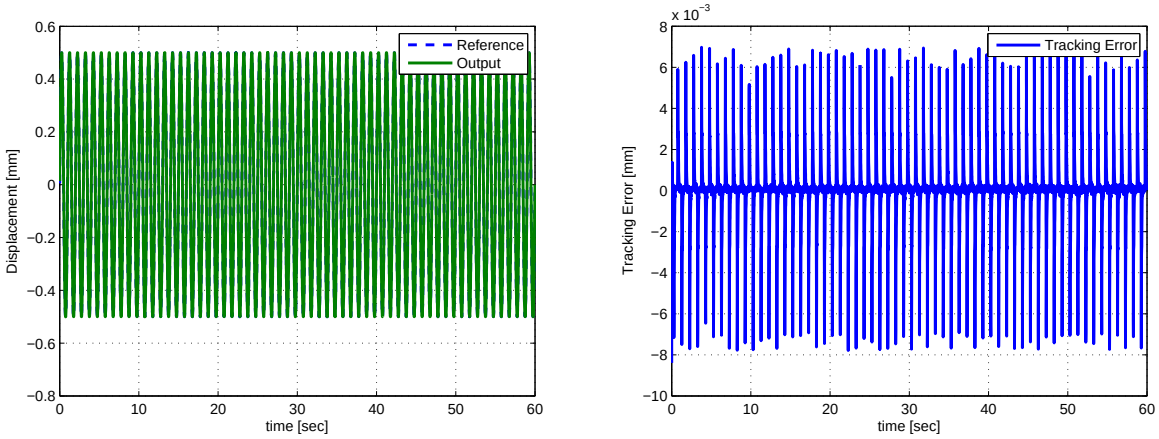

(a) Reference vs output signals: PPI controller experimental.

(b) Tracking error.

Figure 3.11: Experimentally obtained signals.

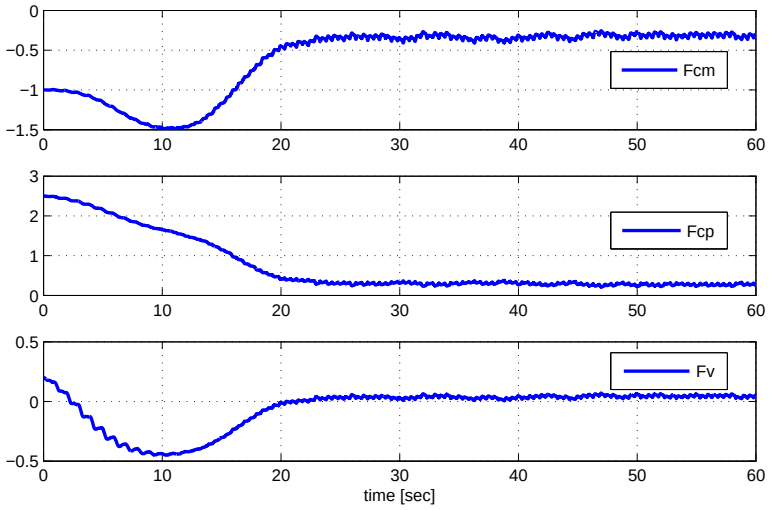

Figure 3.12: Parameter estimation results for adaptive PPI control scheme with static friction model 1: experimental.

3.3.2.2 Static Friction Model 2

For two different scenarios, as mentioned in Section 3.3.1, simulation results are discussed. Sine wave, which has 0.5 amplitude and 1 Hertz frequency, is used as a reference signal. As it illustrated in 3.13.b, there is 0.002 mm tracking error when friction added to the plant. After adaptive control is added to feed drive model, tracking errors go to almost zero after 28 seconds (Figure 3.14). As it can be seen from Figure 3.15, parameters converge their actual values after 40 seconds. Friction change with velocity is also given in Figure 3.16.

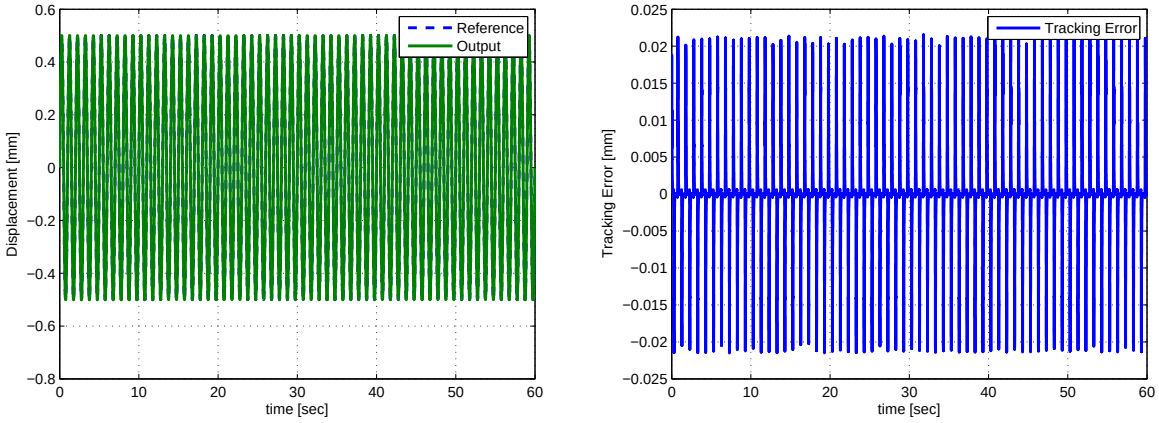

(a) Reference vs output signals.

(b) Tracking error.

Figure 3.13: Non-adaptive PPI control scheme results with static friction model 2.

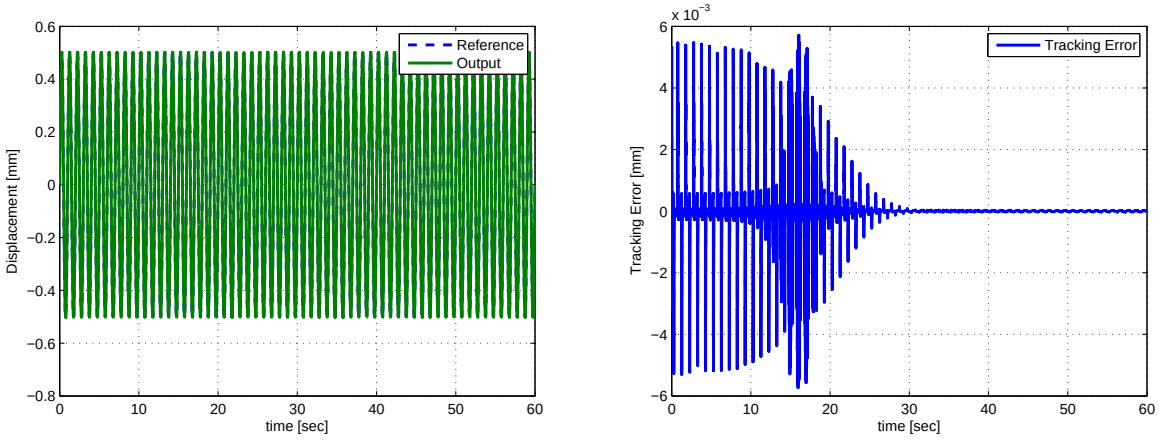

(a) Reference vs output signals.

(b) Tracking error.

Figure 3.14: Adaptive PPI control scheme results with static friction model 2.

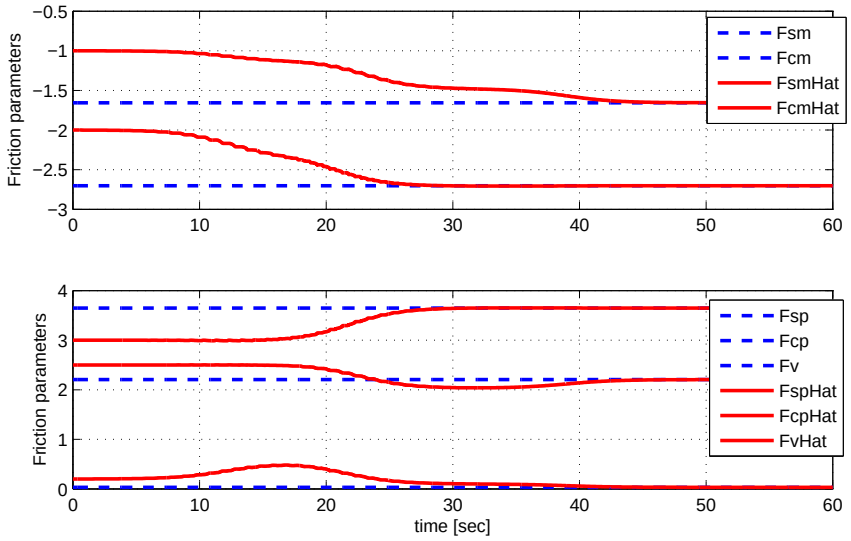

Figure 3.15: Parameter estimation results for adaptive P-PI control scheme with static friction model 2.

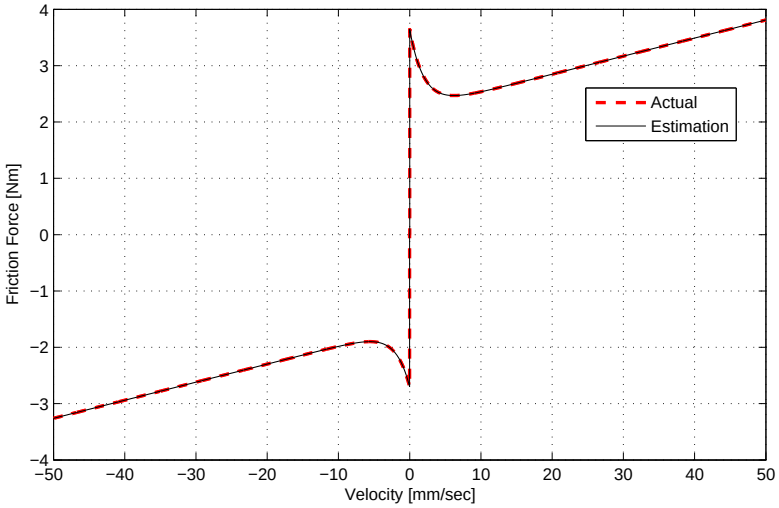

Figure 3.16: On-line parameter identification results at the end of adaptive PPI control run with static friction model 2.

Chapter 4

A Practical Case Study: ODG Grinding Machine

As mentioned in Chapter 2, rigid body construction is easiest way to model feed drive systems. Rigid body models, in general, are combination of inertia affects, viscous damping and friction force. In construction of rigid body model, first step is to identify inertia effects and viscous damping constant. This model can be further detailed considering high frequency flexible modes and nonlinear friction effects, which were summarized in Chapter 2. Chapter 3 had focused on on-line estimation of these latter terms and their adaptive compensation based on the produced estimates, for the cases where the based rigid body model parameters, i.e., inertia and viscosity constant, of the system are available. In this chapter, we focus on off-line identification of these model parameters; we present a real-life industrial case study where such off-line identification is a key problem. This case study was performed as part of an NSERC Engage project with a local manufacturing company, ODG - Ontario Drive & Gear Ltd.

4.1 Motivation and General Problem Definition

ODG is a company that manufactures various types of gears, including marine gears, mining gears, and automotive gears. The company also produces high quality products such as transmissions for various vehicles, power transmission couplings, wind turbines, and conveyor systems. In company, there are different CNC systems such as turning, milling, grinding, and gear shaping machines that allow ODG to achieve optimal precision

of manufactured products (Figure 4.1). During this machining procedures, grinding has a crucial role for gaining fine finish and dimension accuracy. Through this Engage project, main goal is to investigate possible methods of analyzing and predicting accuracy at high speeds during grinding process and developing a high fidelity simulation tool for ODG system.

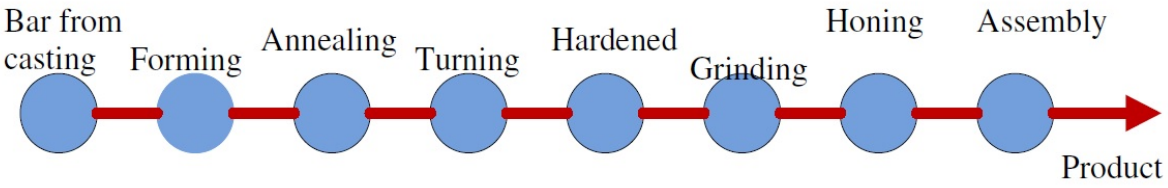

Figure 4.1: Different CNC operations [36].

Typical CNC components are power units, CNC units and mechanical units. Mechanical units consists of feed drive mechanisms. In general, feed drive systems have workpiece, the nut, the ball lead screw etc. The CNC unit has a speed and position sensors, as well as computer unit. The operator gives numerical control (NC) codes to the CNC unit. After processing CNC data, the data is transmitted to the motor with discrete time signals. Motor moves commanded drive and sensors measure velocity and position commands. The CNC unit periodically commits this procedure and feed drive system remain in desired speed and position [1]. Diagram of the grinding machine is given in Figure 4.2. The ring loader takes workpieces from the pallet system and transports these machined workpieces to the workpiece axis. Then, the workpiece is clamped between the workpiece axis and the tailstock. After alignment of workpiece, the infeed axis, the feed axis, and the tool swivel axis move to the machining position and NC program starts sending signals for grinding. The grinding machine is controlled with Siemens 840D controller [37].

Furthermore, there are two kinds of grinding in ODG; form and worm grindings. Main focus on this project was for form grinding. Despite the fact that the form grinding gives high quality gears, it takes 10-15 times more time than worm grinding. If some grinding errors would be decreased by decreasing time with higher speeds, this is going to reduce operational cost.

However, through grinding procedure, dressing of grinding wheel is an important part in order to achieve optimum performance in grinding [30]. During grinding process, it is realized that 20% of the time is spent on dressing cycle. Hence, in this practice case study, the main focus is contributed on dressing cycle during form grinding. During this process, infeed axis (x-axis) and tool shift axis (y-axis) operate together to obtain desired profile

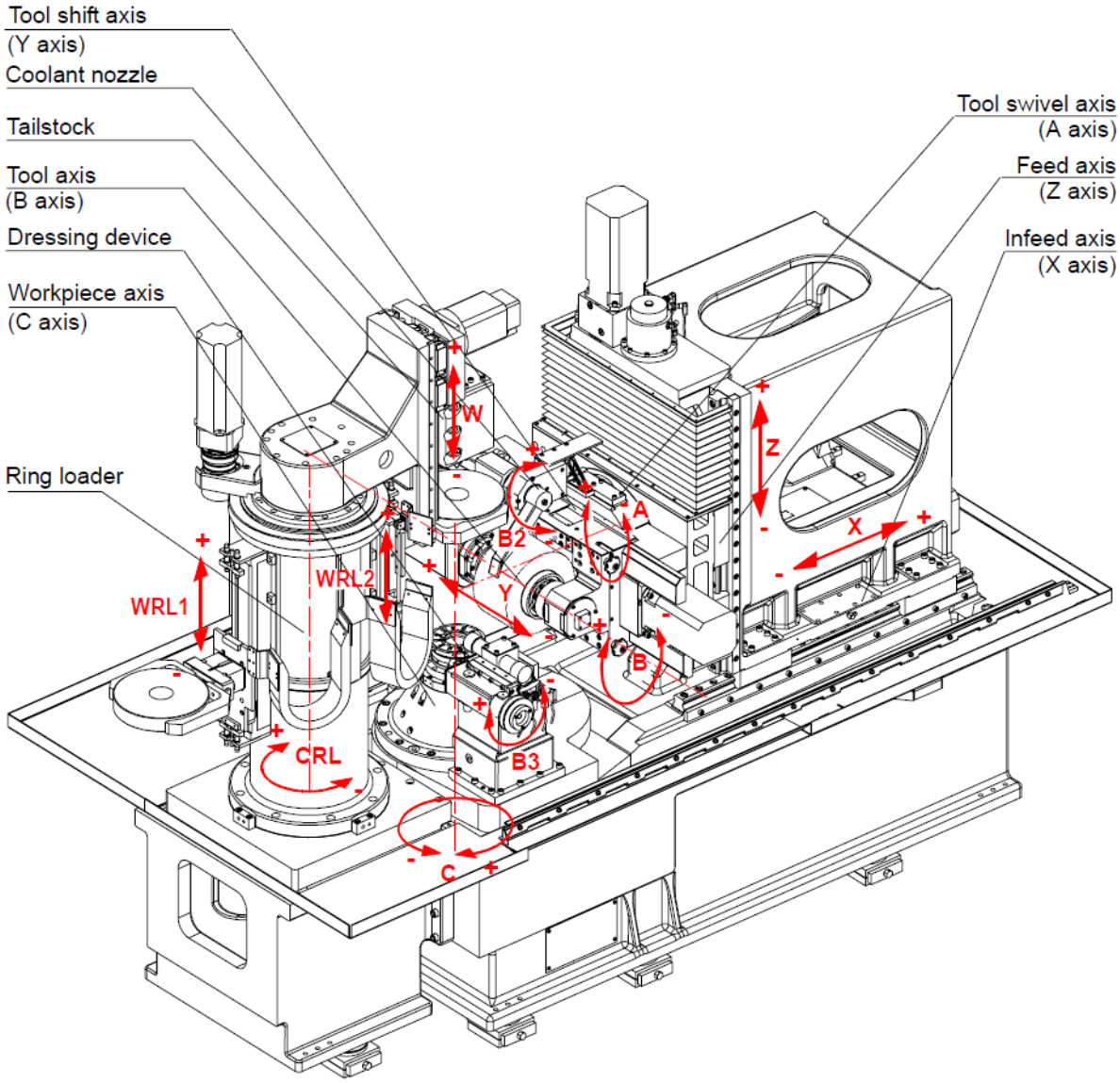

Figure 4.2: Grinding machine diagram [37].

of grinding wheel. Therefore, for these two axes, the rigid body dynamics that includes inertia and viscous friction parameters are identified and the servo controller of the each axis is constructed (Figure 4.3).

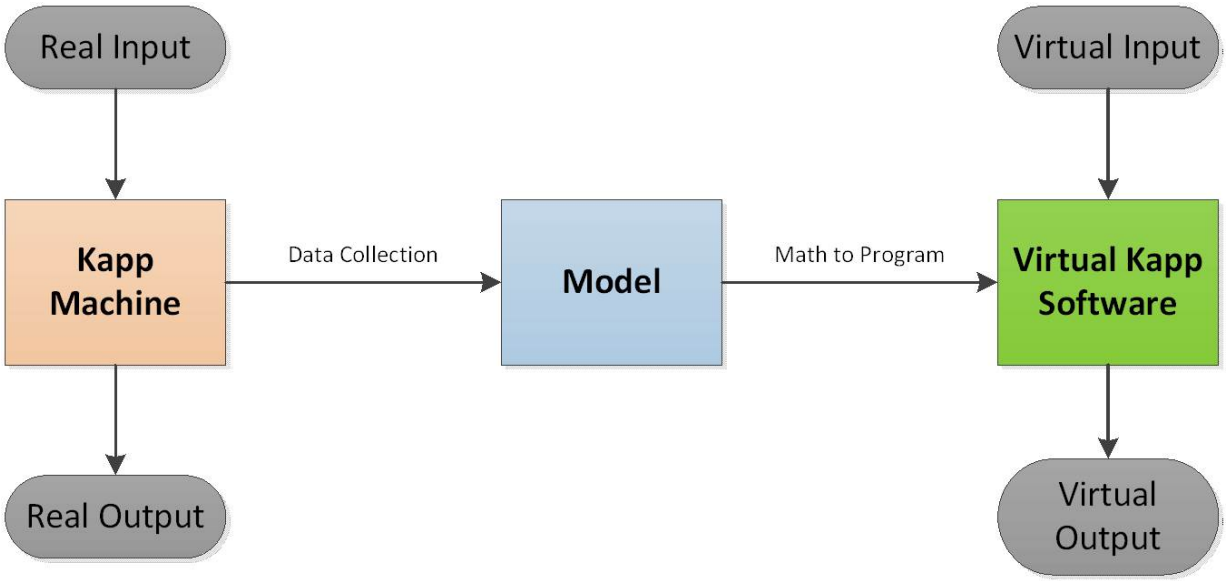

Figure 4.3: Project overview.

4.2 2 Axis Control Structure

Overall controller structure for Siemens controller 840D is given below. In this structure, it should be noted that current controller loop is not taken into consideration. Only position and velocity controller structures are identified. X and Y axes are driven by ball screw

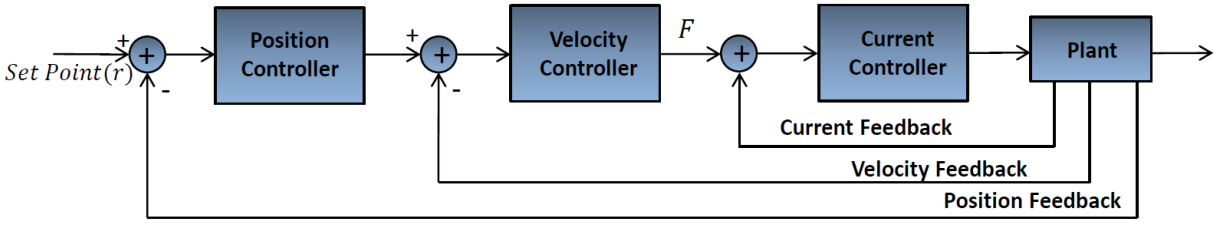

Figure 4.4: General Siemens controller scheme [29].

drives. X axis is in radial direction with respect to the workpiece. Y axis moves axially by means of the tool shift axis (Figure 4.2). During dressing cycle, infeed and tool shift axes move toward positive and negative direction to form grinding wheel. The rigid body dynamic modeling is the easiest way to represent effect of inertia, viscous and Coulomb type friction terms. More advanced modeling which including vibrations, more complicated

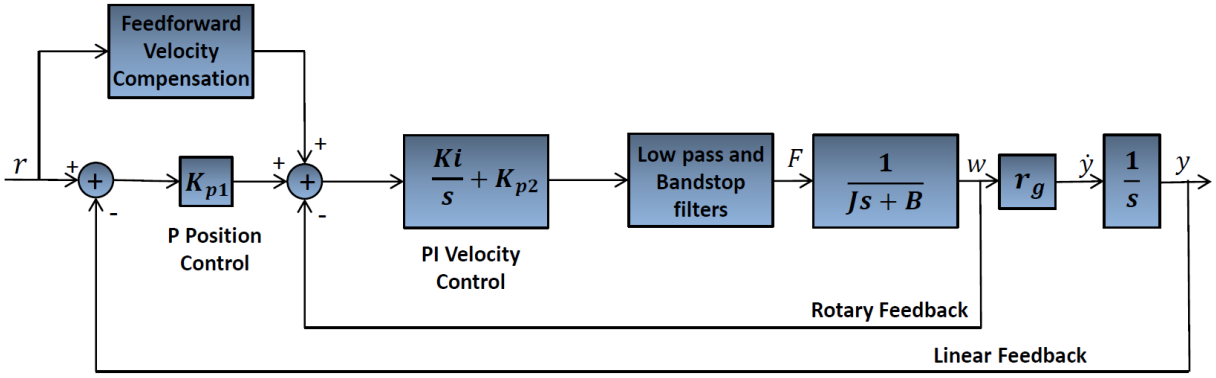

Figure 4.5: Dynamic model representation of X and Y axes.

nonlinear friction effect, motor torque ripples etc. would help to represent the behavior and predict the response more precisely. In this study, we prefer using the rigid body modeling for a couple of reasons: (1) As mentioned, the simplified rigid body model captures the major components of the dynamics for typical operation conditions of the CNC machines (e.g., at ODG) during manufacturing processes. (2) We need a simplified model as opposed to a complicated one for parametric modeling, identification, and simulation purposes. (3) Production of more detailed models and reliable incorporation of them with identification and control schemes require a longer time span than that of the aforementioned NSERC Engage project and this thesis study; they are beyond the scope of the project and thesis as well. The linear dynamic model of the Figure 4.5 apply to both of X and Y axes. In this widely used dynamic model, it should be noted that the feedforward speed compensation term is not taken into consideration for this study.

4.3 Frequency Domain Analysis and Offline Identification

In this section, our studies on open loop and closed loop identification of the key rigid body model parameters and the built-in controller parameters of the grinding machine of interest are presented. In the first part of the section, inertia and viscous damping coefficient's identification will be given. Afterwards, PI velocity loop identification by using frequency domain measurements and position control loop gain identification using time measurements will be described. As it is demonstrated in Figure 4.5, in the closed loop,

low pass and bandstop (notch) filters are used. Equation of this filters and explanations will be discussed at the end of this section.

4.3.1 Open Loop Identification of Plant

Open loop frequency response data was collected. The collected data refers to as a measured quantity speed actual value/torque actual value as it can be seen from Figure 4.6. Then, the equivalent inertia and viscous friction coefficients were identified. Normally, the both axes motor inertia is $J = 0.0048\ kgm^2$. Yet, the equivalent inertia of the system is generally 2 to 4 times greater than motor inertia. The reason is that in addition to the motor mass, there are also the other components of the ballscrew drive such as table and ballscrew mass that effects the overall inertia with respect to the motor shaft.

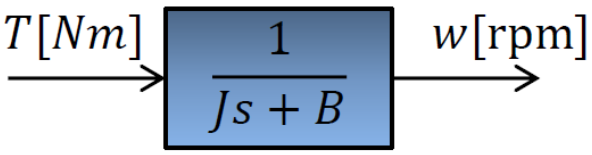

Figure 4.6: Open loop scheme.

As demonstrated in the Figure 4.7 and 4.8, there is no reasonable match between identified and experimental models until 100 Hz for both X and Y axes. This may be because of the friction effect. In addition, the viscous friction coefficient is not taken into account since it's affect is too small. After this point, the results seem to be matched. From 350 Hz to 1000 Hz, there is vibration in the system and since rigid body gives reasonable results for low frequencies, this is taken as an expected outcome.

4.3.2 Closed Loop Identification

4.3.2.1 Closed Loop Identification of Velocity Loop

In this section, closed loop response of experimental data is analyzed. A lot of controller structures are used in the manufacturing industry in order to avoid stability issues and get the desired dynamic performance. One of them is to plug a velocity loop within the position loop, as it can be seen from Figure 4.5. This overall system called P-PI control. This controller is used for two reasons; it is simple to implement and easy to tune for

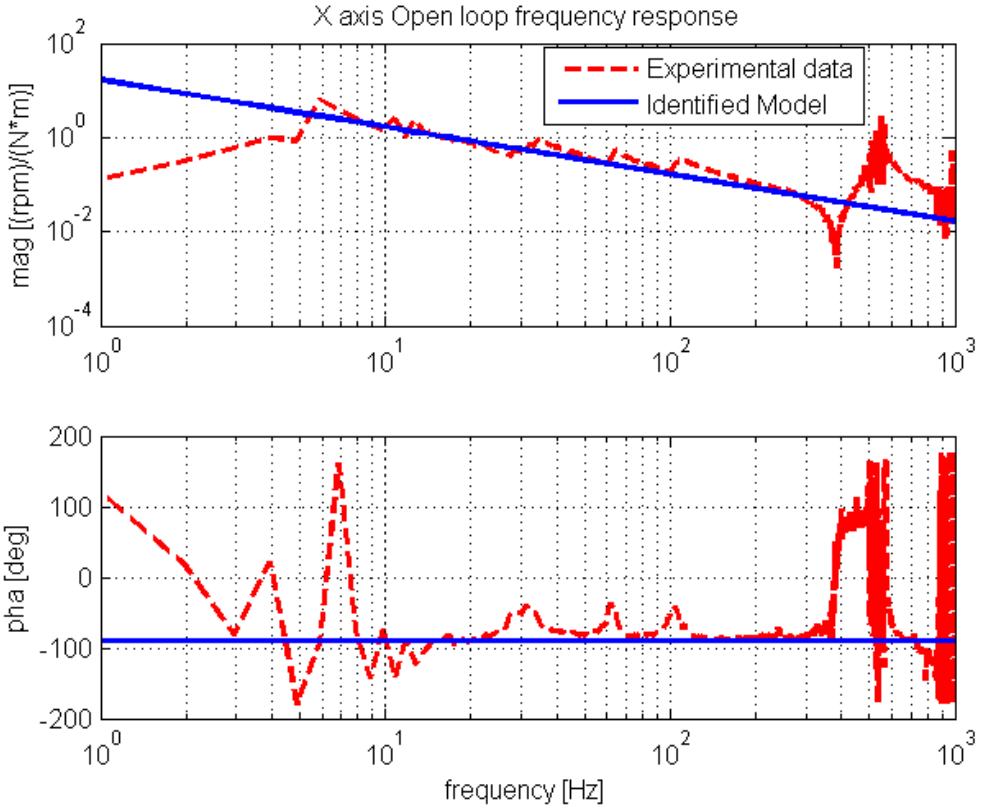

Figure 4.7: X axis open loop response.

complicated systems. This controller is also built in controller structure in the grinding machine digital controller.

As a first step of identifying velocity (PI) controller, controller transfer function is derived by using open and velocity closed loop transfer functions. Controller transfer function is (Figure 4.9),

$$G_c = G_v G_f$$

where G_v is velocity(PI) controller transfer function and G_f is filter's transfer function. For the velocity loop, if we call overall velocity loop transfer function G_{cv}, we can find G_c as,

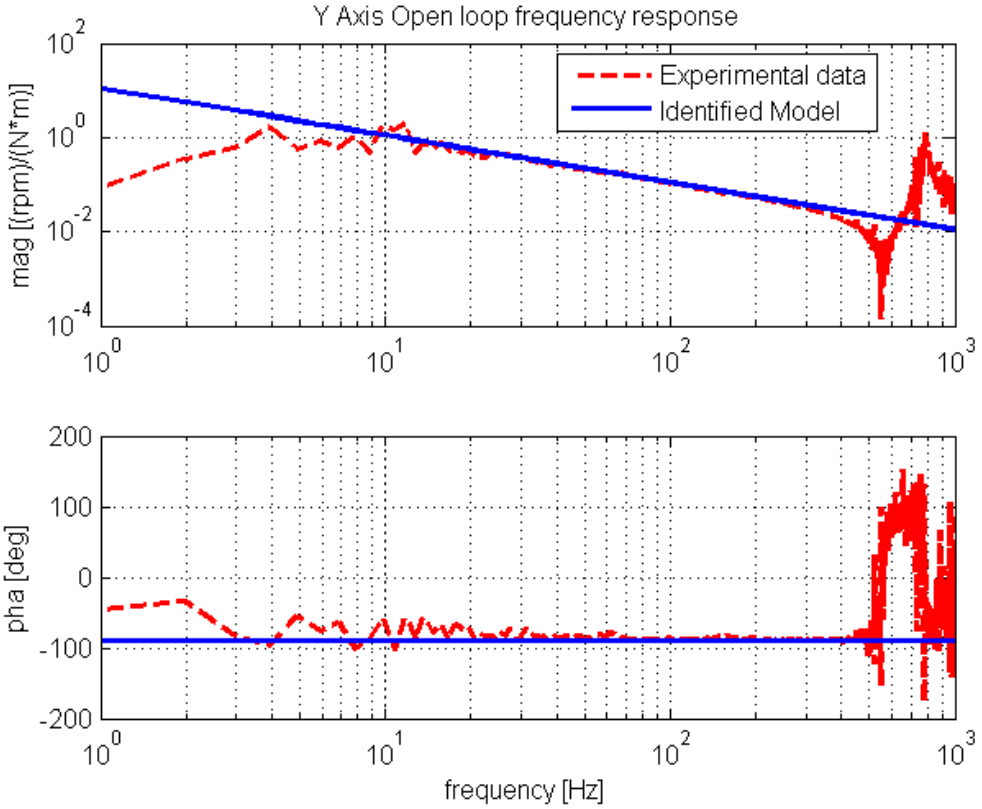

Figure 4.8: Y axis open loop response.

$$G_{cv} = \frac{G_c G_p}{1 + G_c G_p} \quad \rightarrow \quad G_c = \frac{G_{cv}}{G_p - G_{cv} G_p}$$

To identify G_{cv} and G_p, velocity closed loop and open loop experimental responses are considered. Using this point of view, controller experimental response can be found, which we are going to call this estimated controller response. In the Figure 4.10 and 4.11, mathematically derived model (G_p) and estimated controller frequency analysis can be seen. Estimated response is constructed in order to check if controller gains are chosen properly. There is a reasonable match between both frequency responses. It should be noted that grinding machine manufacturer also provided a actuator amplification factor (f_a) that needs to be taken into account inside the closed loop. This factor's mathematical

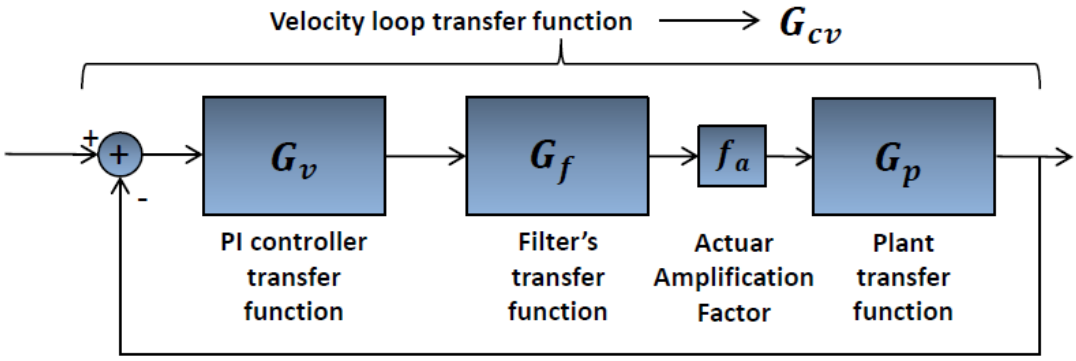

Figure 4.9: Illustration of transfer functions.

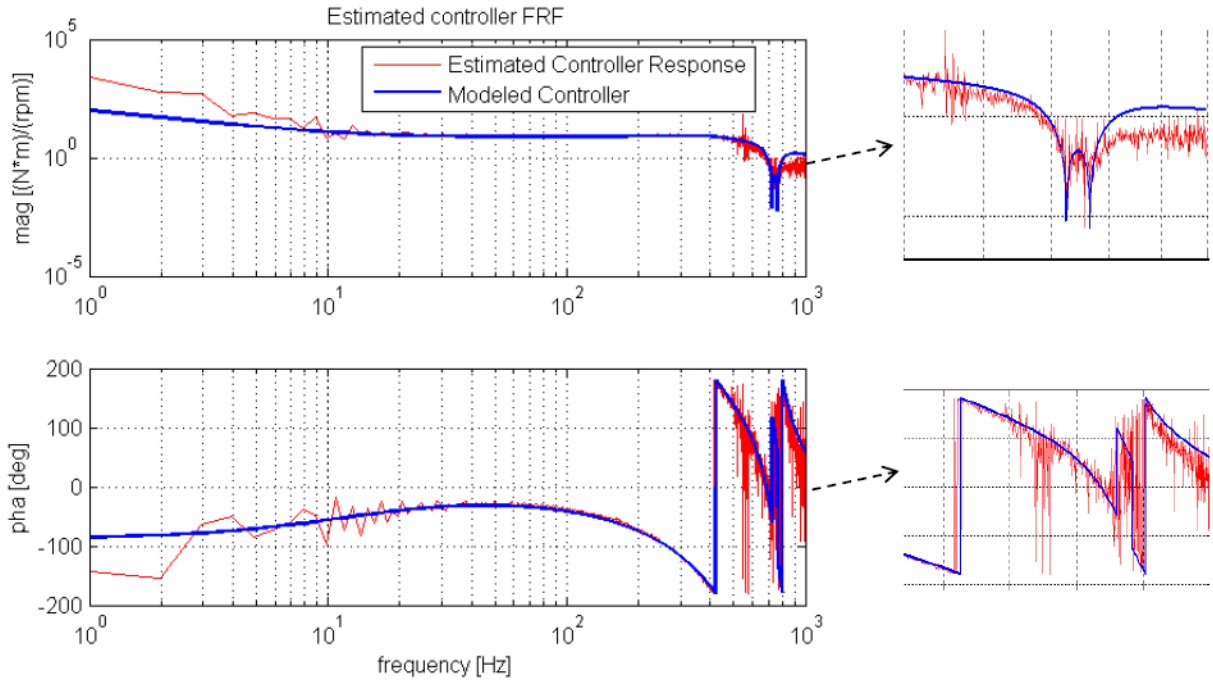

Figure 4.10: Controller identification for Y axis.

expression also given below.

$$n_{motor} = \frac{r_{mn}}{r_{md} h_g} \qquad [rpm]$$

Here, n_{motor} refers to motor speed. r_{mn} and r_{md} are number of motor and spindle revolution,

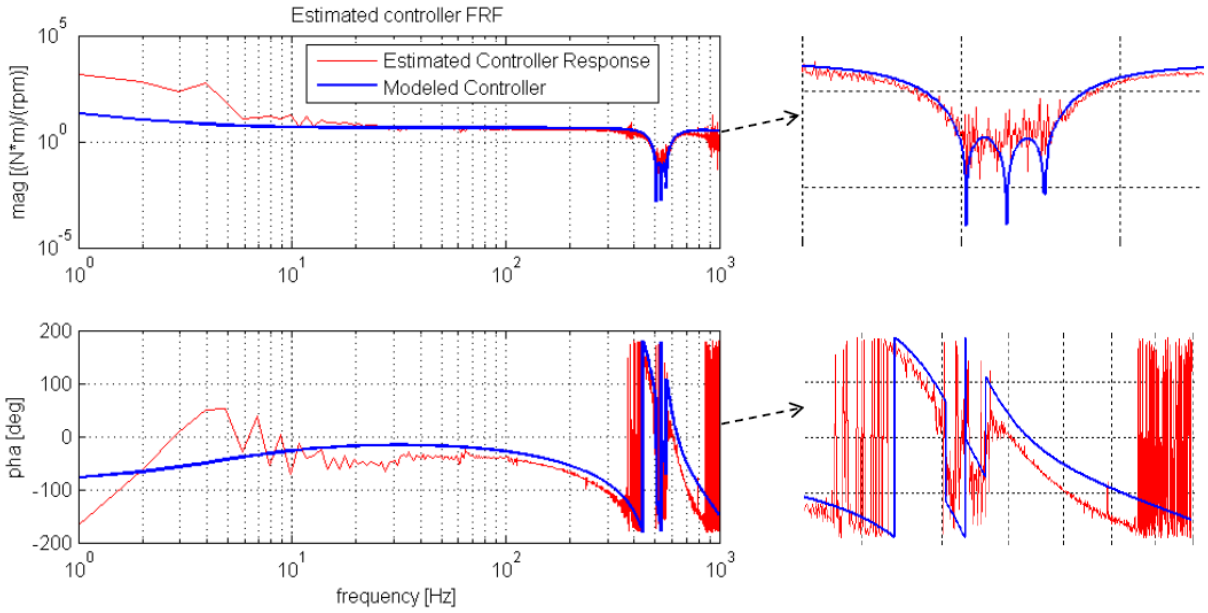

Figure 4.11: Controller identification for X axis.

respectively. In addition, h_g represents the lead screw pitch length.

$$f_a = \frac{n_{motor} 14.8}{C_i K_t}$$

where C_i is motor maximum current and K_t is torque current ratio.

4.3.2.2 Closed loop filters

As a first step of system control, it is expected to do some changes in the system it self such as adding damping or stiffness to the structure to obtain desired dynamics. In addition, adjusting the controller gains and getting sufficient design might be restricted to some specified limits. Therefore, adding the system filters would be the best way of achieving satisfactory design because it has simple structure and effective performance [31]. In general, bandstop filters are used when some disrupted frequencies are pretty strong, or high attenuation is needed at particular frequencies. On the other hand, low pass filters are used to alleviate the signal when there is a higher frequencies than cutoff frequency. In the grinding machine, for Y axis, four second order low pass and four bandstop (notch)

filters are used. On the other hand, there are two low pass filters and four notch filters available for X axis. The transfer function of the filters are given below.

Low pass filter structure;

$$G_{lp} = \frac{w_{lp}^2}{s^2 + 2\zeta w_{lp} + w_{lp}^2} \tag{4.1}$$

Low Pass Filters	**X Axis**	
	Damping	**Natural Frequency [Hz]**
Filter 1	0.7	2000
Filter 2	0.7	1100

Table 4.1: Low pass filter specifications for X axis.

Low Pass Filters	**Y Axis**	
	Damping	**Natural Frequency [Hz]**
Filter 1	0.5	450
Filter 2	0.7	2000
Filter 3	0.7	2000
Filter 4	0.7	2000

Table 4.2: Low pass filter specifications for Y axis.

Here, ζ is damping ratio and w_{lp} is natural frequency for low pass filter. Parameter values of low pass filters are given in Table 4.1 and 4.2.

Bandstop (Notch) filter transfer function;

$$\begin{aligned} G_{bs} &= \frac{s^2/(2\pi f_z)^2 + s(2\pi f_{bz}/(2\pi f_z)^2) + 1}{s^2/(2\pi f_n)^2 + s(2\pi f_{bn}/(2\pi f_n)^2) + 1} \\ &= \frac{s^2/(2\pi f_z)^2 + s(2D_z/(2\pi f_z)) + 1}{s^2/(2\pi f_n)^2 + s(2D_n/(2\pi f_n)) + 1} \end{aligned} \tag{4.2}$$

Here, D_z and D_n are numerator and denominator dampings, respectively. f_z represents the blocking frequency and $f_n = (MD_{1222})f_z$ refers to bandstop natural frequency, where (MD_{1222}) (percent) is used to decrease the amplitude for frequencies above the blocking frequency. $f_{bz} = 2D_z f_z$ is numerator bandwidth and $f_{bn} = 2D_n f_n$ is denominator bandwidth. Parameter values of band stop filters are given in Table 4.3 and 4.4.

In conclusion, the closed loop response of velocity loop for X and Y axes is given in the Figure 4.12 and 4.13. Blue colored signal is constructed by using open loop experimental

Bandstop(Notch) Filters	X Axis			
	$f_z[Hz]$	$f_n[Hz]$	$f_{bz}[Hz]$	$f_{bn}[Hz]$
Filter 1	505	505	0	120
Filter 2	535	535	0	180
Filter 3	565	565	0	120
Filter 4	3500	3500	0	500

Table 4.3: Bandstop filter specifications for X axis.

Bandstop(Notch) Filters	Y Axis			
	$f_z[Hz]$	$f_n[Hz]$	$f_{bz}[Hz]$	$f_{bn}[Hz]$
Filter 1	3500	3500	0	500
Filter 2	725	725	0	150
Filter 3	765	765	0	150
Filter 4	3500	3500	0	500

Table 4.4: Bandstop filter specifications for Y axis.

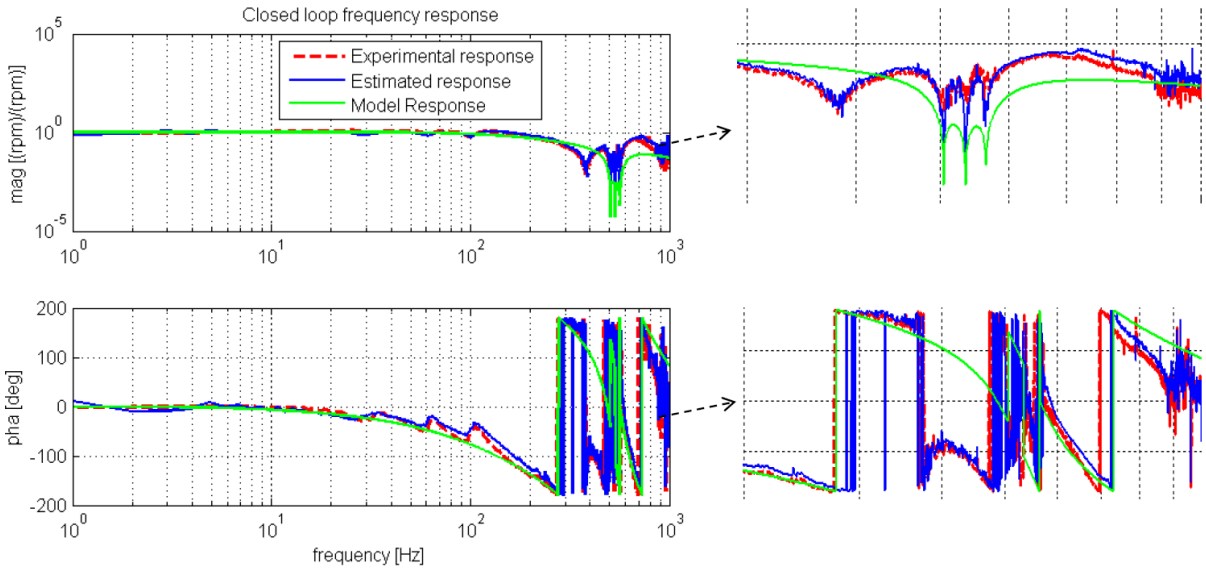

Figure 4.12: Closed loop response for X axis.

and mathematically derived PI controller, which is called estimated response. This is done in order to check if controller gains are tuned properly. Mathematically modeled and simulated response is given with green colour. Experimental response of velocity closed loop dynamis is also illustrated with red colour. As it demonstrated, because of the rigid

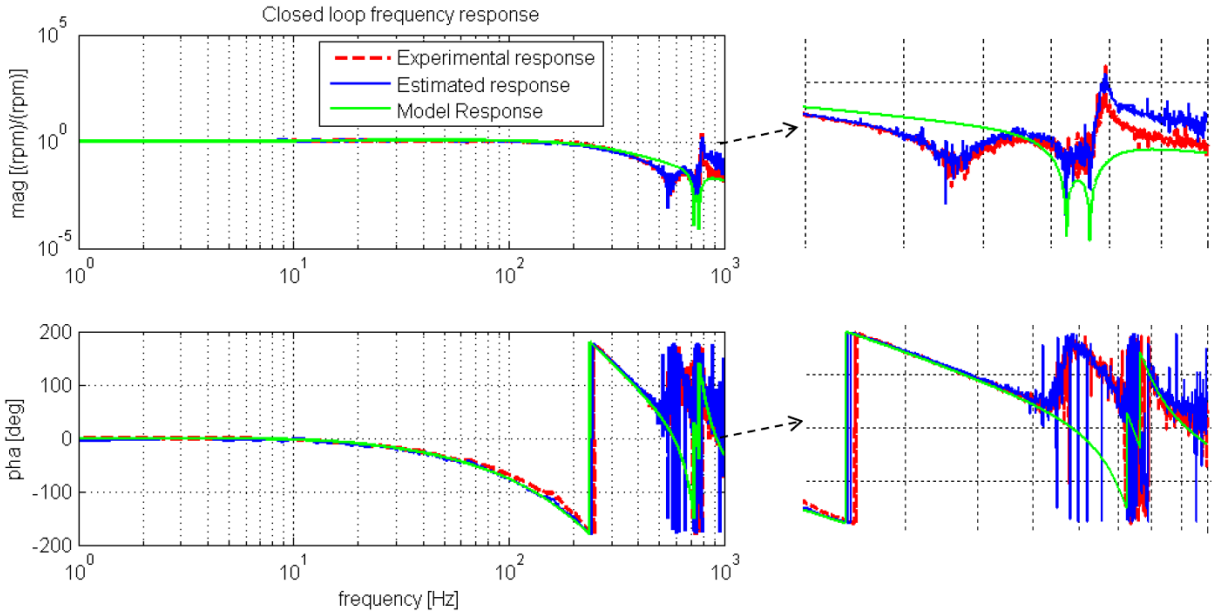

Figure 4.13: Closed loop response for Y axis.

body dynamics, there is almost perfect match for low frequencies. After 350 Hz, there is notably difference between modeled and experimentally obtained responses. This is because of resonances and unmodeled dynamics.

4.3.2.3 Closed Loop Identification of Position Loop

In order to find closed loop gain (K_{p1}) and finalize the mathematical model of overall transfer function, time measurements are used. Figure 4.14 and 4.15 are the reference trajectories for X and Y axes. However, it should be noted that while analyzing simulation in virtual environment such as matlab, noisy signals sometimes might cause misinterpretation of the analysis. In order to overcome this problem and get rid of some part of noisy measurements, reference and output trajectories are passed through 6th order butterworth filter. In addition, 500 Hz cutoff frequency and 1500 Hz nyquist frequency, which is half of the sampling rate are used for this filter. Obtaining of time measurements will be explained in detail in section 4.4.

Figure 4.14 and 4.15 are reference signals that applied to the each axis. X and Y axes go back to their original started position after 20 seconds. Filtered actual signals from experimental setup for X and Y axes are given in the Figure 4 16. As expected, there

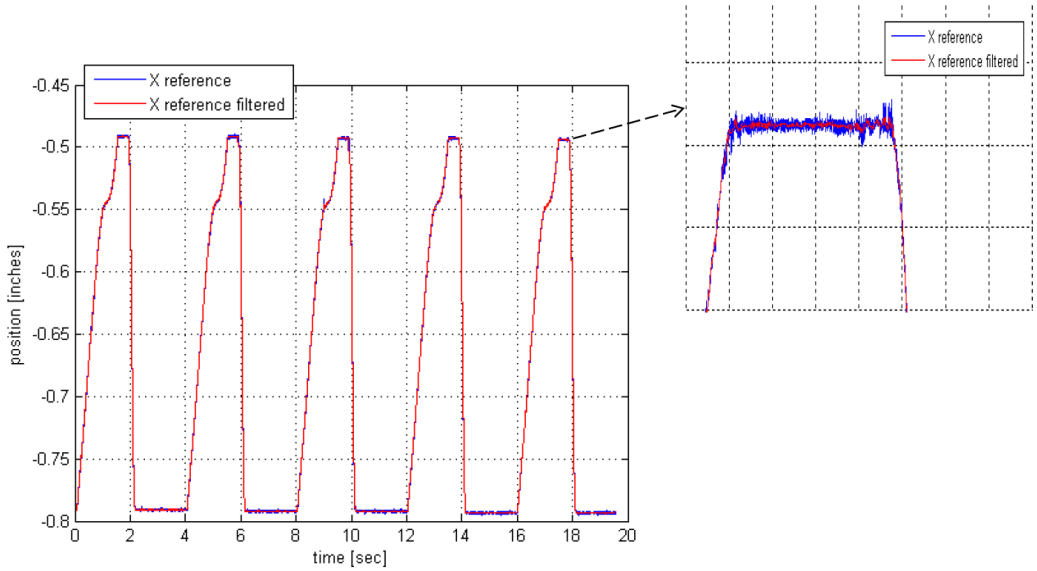

Figure 4.14: X axis reference signal.

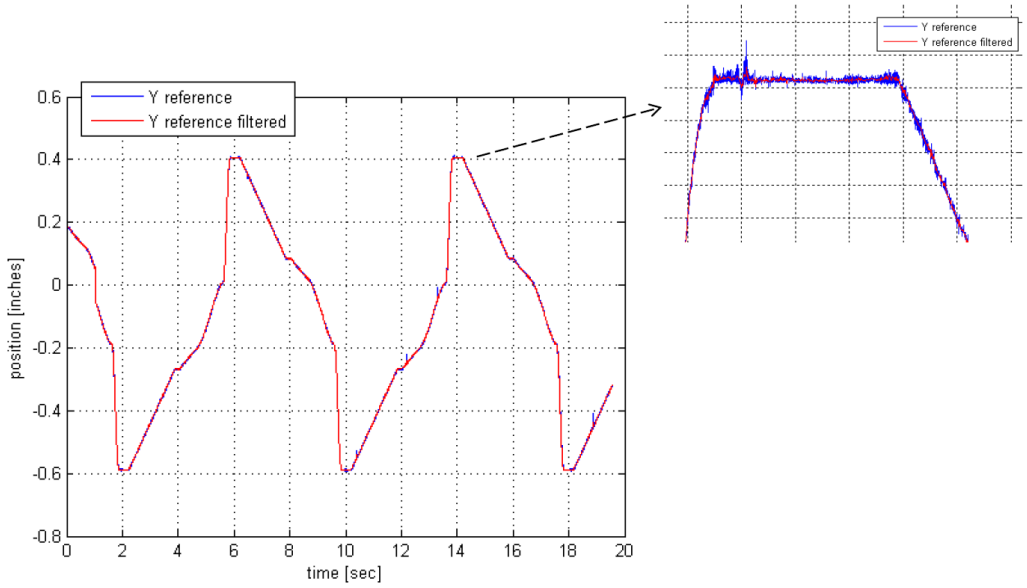

Figure 4.15: Y axis reference signal.

are more noise than reference signals. Tracking error for X axis is over 0.002 inches, but

there are peaks during turning the corners. On the other hand, for Y axis, tracking error goes 0.005 inches after 2 seconds and there are also some peaks in the corners of the signal (Figure 4.17).

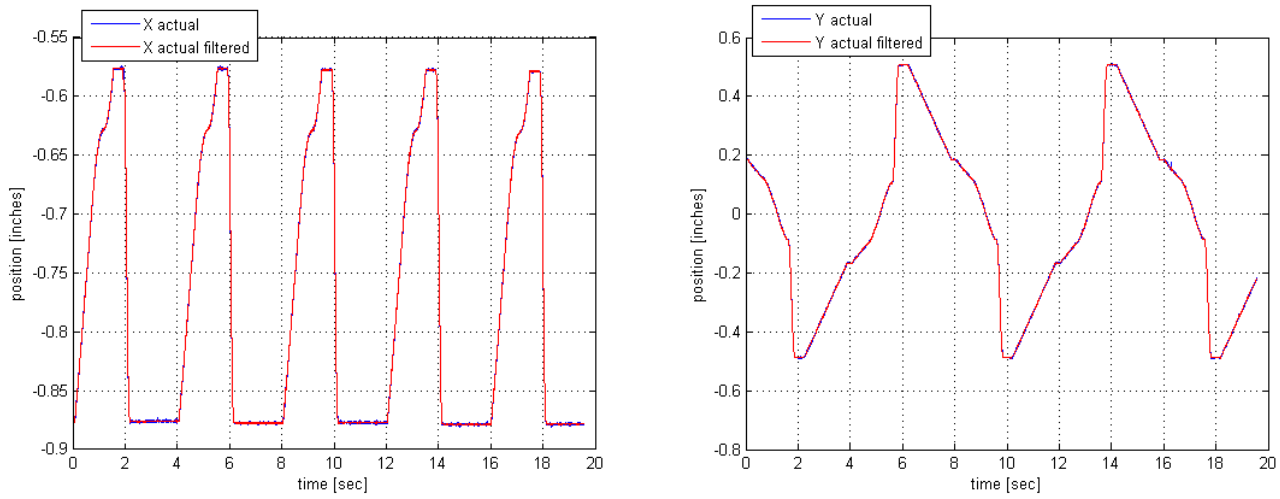

(a) X axis actual.

(b) Y axis actual.

Figure 4.16: Actual signals.

Figure 4.18 shows the Y vs X axes position experimental measurement result. Dressing cycle takes around 20 seconds. In three periodic movements of X and Y axes, dressing procedure is completed. At the end of the cycle, dressing wheel is formed as desired. This result is constructed by considering one dressing cycle of the movement during grinding.

Simulation Results: In order to find position control gain (K_{p1}), simulation output signals are compared with experimental measurement outputs given in Figure 4.16. Figure 4.19 and 4.20 show the output signals obtained from simulations. Tracking errors are close to experimentally obtained signal's tracking (Figure 4.17, 4.19 and 4.20). Figure 4.21 illustrates actual signal from experiment and output signal from simulation. Signals are tuned to be as close as possible to each other in order to find proportional gain.

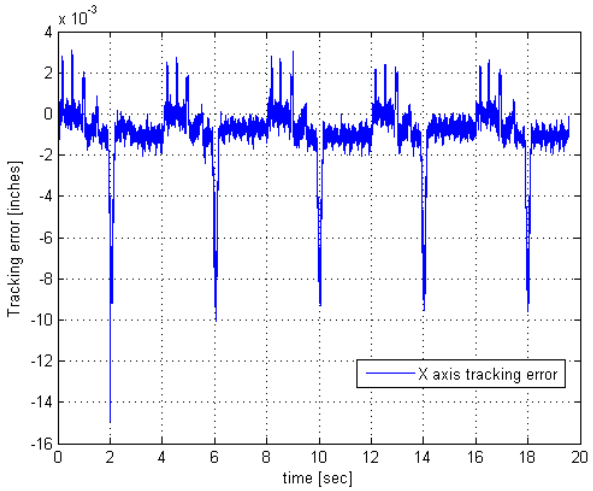

(a) X axis tracking error.

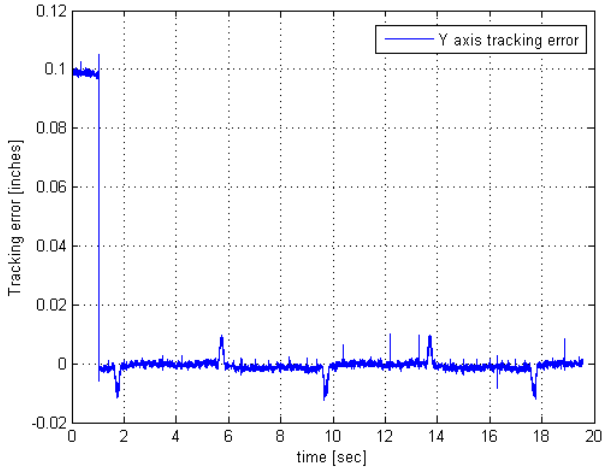

(b) Y axis tracking error.

Figure 4.17: Tracking errors of X and Y axes.

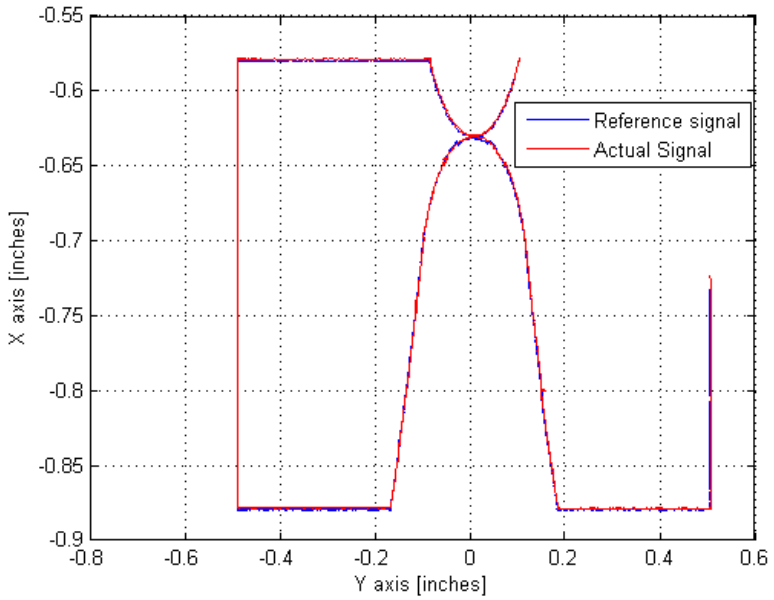

Figure 4.18: Trajectory during dressing cycle.

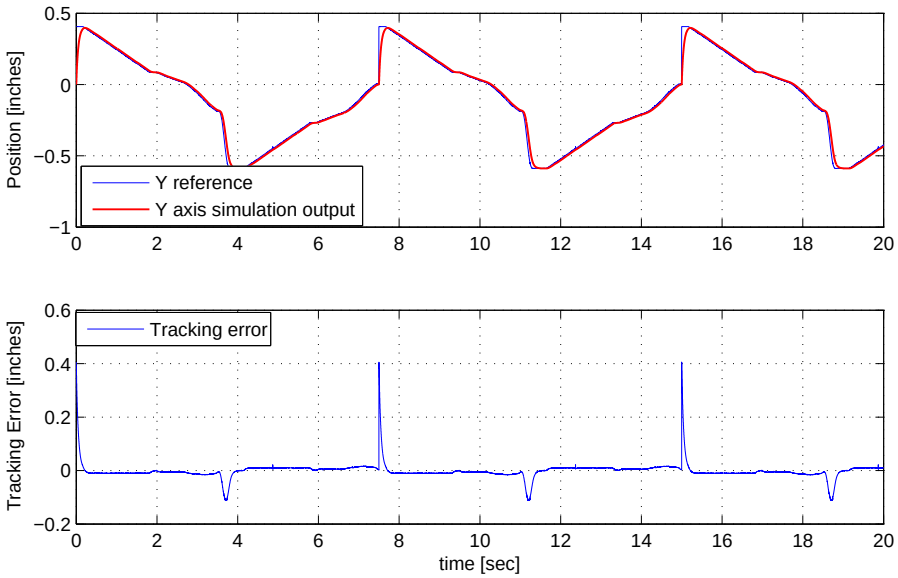

Figure 4.19: Y axis simulation.

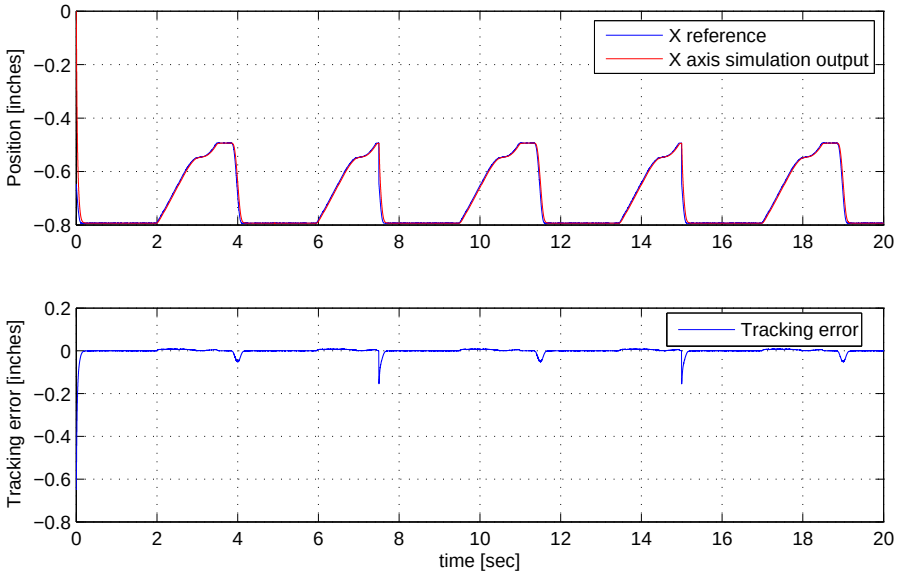

Figure 4.20: X axis simulation.

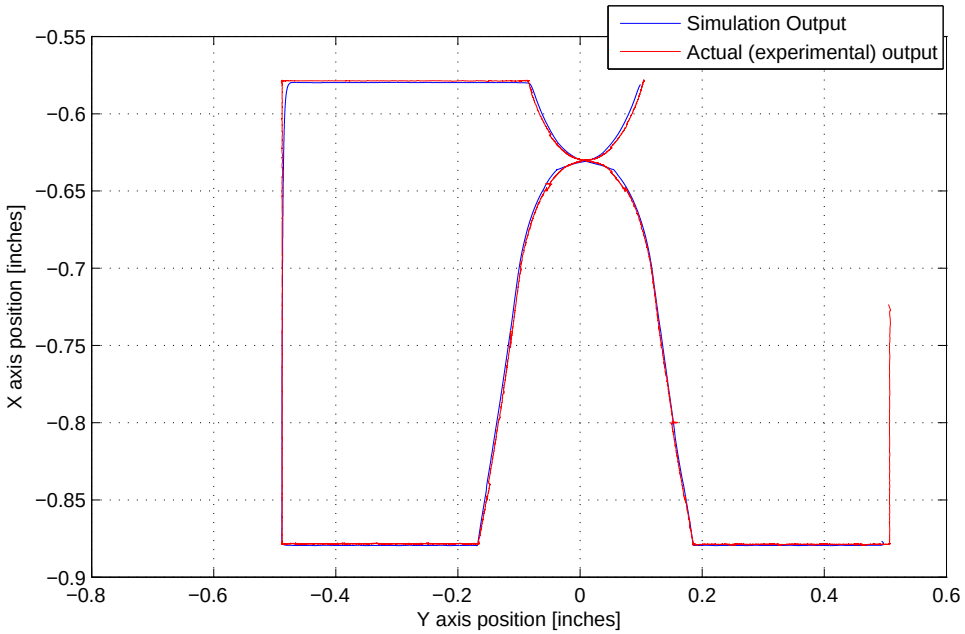

Figure 4.21: Simulation output vs experimentally obtained actual signals.

4.4 A High-Fidelity Simulation Tool for ODG System

In order to construct mathematical model of each axis dynamic, time measurements are needed as it mentioned above. Time measurements are collected by using Siemens digital to analog converter (DAC). The device for collecting time measurements is built and implemented by Ivan Chan. Measurement results are also investigated with the Cooperation of this Coop student in University of Waterloo.

In Siemens 840D, there are three channels available for giving preselected signals, which is ranging from 0 [V] to +5 [V]. Sampling rate was also over 3 kHz. However, here, voltage unit corresponds to physical units while looking at the signals. For example, 1 V = 5 mm means the axis is placed 5 mm from original position. Henceforth, all voltage units are first converted to their actual units. In addition, there were some restrictions during obtaining the output signals. Since signal was restricted between 0 and 5 V, all signals are reconstructed. Rebuilt and reconstructed signals can be seen in Figure 4.22.

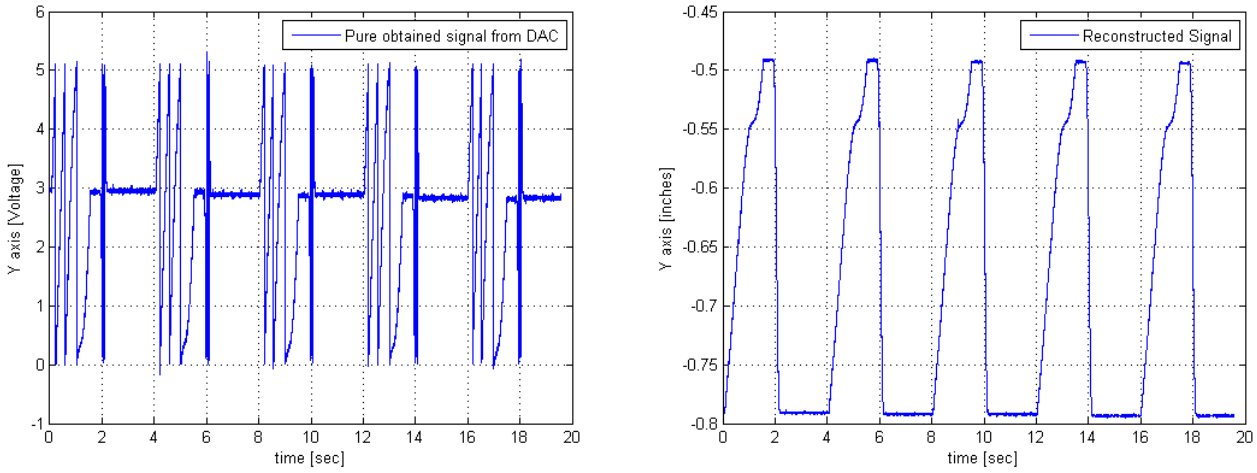

(a) Signal without reconstruction.

(b) Signal with reconstruction.

Figure 4.22: Signals from DAC.

4.4.1 Data Acquisition Unit (DAU)

Data acquisition unit is used in order to convert the analog output signals from ODG grinder machine into the digital signals. These signals are helped us to collect data and

further implement on a computer. For this purpose, National Instrument NI USB-6210 data acquisition unit is used. DAU unit allows us to download data from five controllers at the same time and each controller contains three DAC channels. National Instrument data acquisition unit is also capable of interacting with .NET programming languages such as C#. Data acquisition software is constructed in C# to obtain signal from DAC unit (Figure 4.20). Data is collected and saved as .csv format and exported to Matlab.

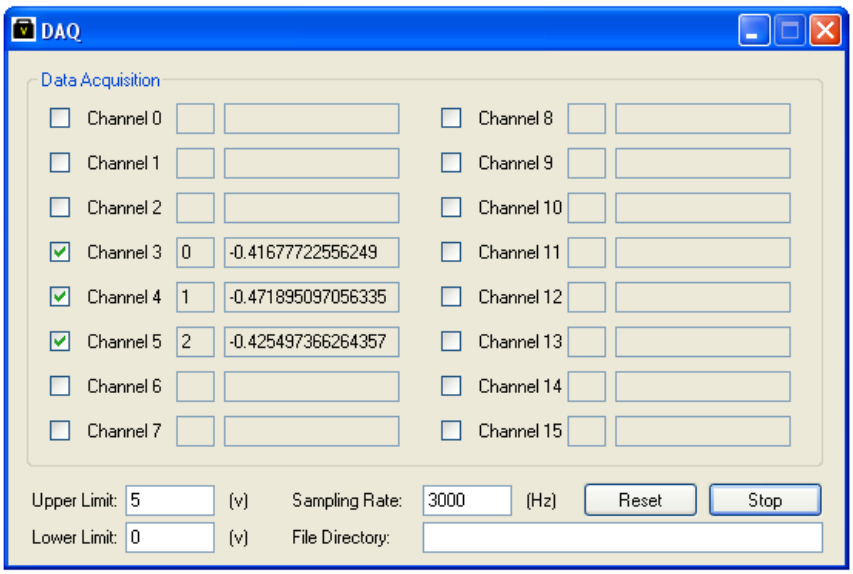

Figure 4.23: Data Acquisition unit C# interface.

4.4.2 Machine Modeling and Simulation

As can be seen from Figure 4.24, frequency analysis of each axis is conducted by collecting measurements from grinding machine as mentioned in Section 4.3. After identification of closed loop system, X and Y axes position set points and actual position signals were collected. It should be noted that these data collection processes are repeated until achieving satisfactory design. After sending collected data files as .csv format, dynamic models of each axis is built in Simulink as mentioned above. Simulink output signals are compared with actual signals from grinding machine. Dressing wheel form is found as in Figure 4.25 after designing Matlab models for each axis. Afterwards, this wheel shape is used in 3D simulation software to see the gear errors (Figure 4.26).

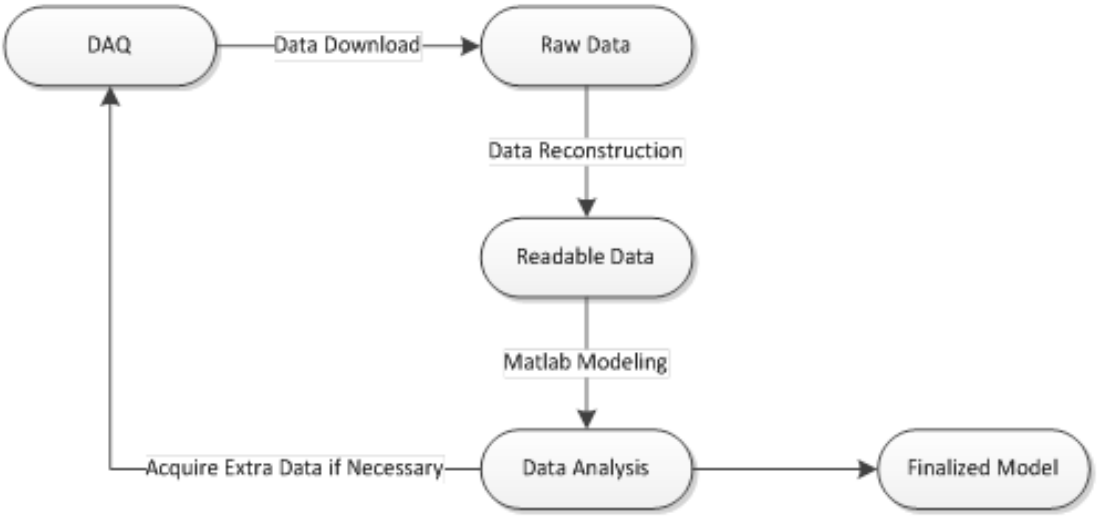

Figure 4.24: Overall work scheme.

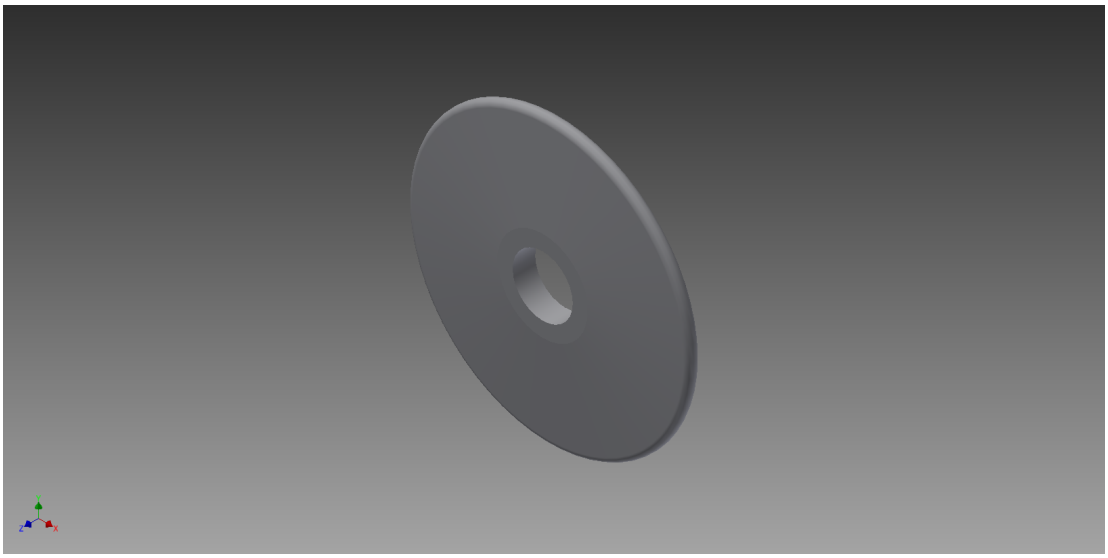

Figure 4.25: Dressing Wheel.

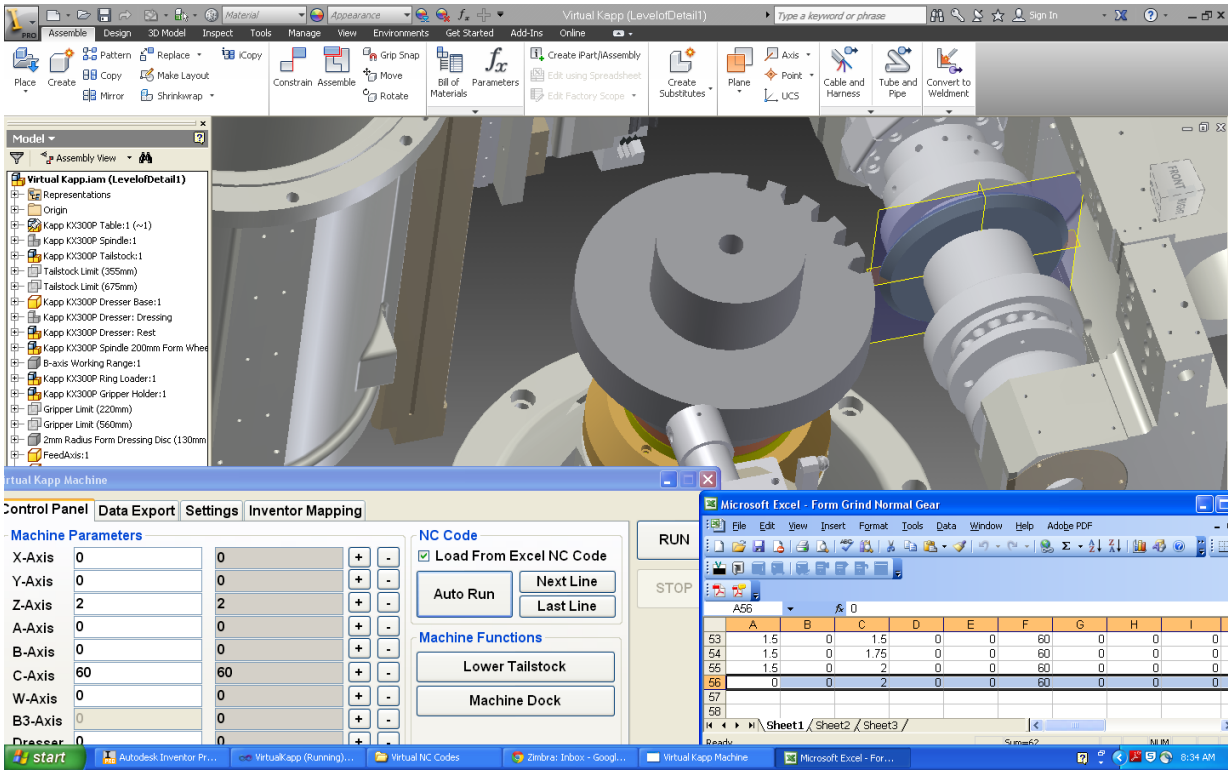

Figure 4.26: 3D simulation of form grinding.

Chapter 5

Discussions and Conclusions

In Chapter 3, based two widely used classical (static) friction models, a least squares on-line friction estimator and an adaptive friction compensation scheme have been designed. The performance of the developed on-line estimator and adaptive control scheme have been evaluated via simulation and experimental tests. In adaptive control design, two different feedback approaches have been used; (i) a new backstepping control design based on constructive Lyapunov analysis and (ii) a classic P-PI control approach. In both simulations and experimental tests, it has been observed that on-line parameter estimation algorithms and adaptive control schemes have achieved desired performance, diminishing most of the friction effects.

During simulation and experimentation, some of the parameters of the classical friction models that can change for different systems were assumed to be available. For the cases where these parameters are unavailable, the designed adaptive control laws and on-line estimation methods can be modified as a future work. Furthermore, as discussed in Chapter 2, most of the dynamic models are nonlinear in parameter. It is therefore challenging to fit dynamical models into SPM form. For further work, using more detailed friction models such as the Lueven or the Maxwell slip models and then developing on-line estimation and adaptive law algorithms is expected to increase friction compensation performance. Hence, most of the undesired friction effects can be eliminated from the system of interest, using dynamical friction models. In addition, the tracking errors due to friction can be further reduced following a direct adaptive control approach.

In Chapter 4, practical case study for finding rigid body model parameters (inertia and viscosity constants) and the parameters of the built-in controller are explained. Real-time experimental measurements have been collected from grinding machine in Ontario Drive

& Gear company. Rigid body model designs have been constructed based on dressing cycle during grinding machining procedure, noting that the cycle takes 20% of the process time for grinding. Dynamic model designs have been constructed for two axes that are active during dressing, namely X and Y axes. X and Y axis dynamic systems have been identified, including rigid body plant, velocity and position controllers, and low pass and band stop (notch) filters within the built-in controllers. Velocity loop identification has been performed based in frequency domain, and the position loop has been identified using time measurements of the two axes. Finally, 3D model of the CNC grinding machine has been developed integrating using experimentally developed dynamic model of two axes.

For the practical case study, identifying feed drive dynamic parameters, finding controllers, and constructing mathematical model is just the first step of analyzing and enhancing the system. For future work, different friction models are planned to be used in the axis dynamics. Various compensation techniques can be built for further works for grinding machine. Rigid body model can be improved by taking into account external forces, torque ripples to the system. In addition, since there are resonances in the system for high frequencies, modeling these vibrations will allow us to get closer results to the actual system dynamics. In addition, 3D model simulations of the grinding machine have been obtained by constructing dressing wheel shape with Matlab based analysis. X and Y axis dynamics identification and simulation can be improved and dressing cycle time can be reduced without sacrificing precision of dressing wheel by constructing a more detailed virtual CNC machine, and correlating X and Y axes dynamics with this virtual design.

References

[1] Y. Altintas. *Manufacturing automation*. Cambridge University Press, 2012.

[2] B. Armstrong-Hélouvry, P. Dupont, and C. Canudas De Wit. A survey of models, analysis tools and compensation methods for the control of machines with friction. *Automatica*, 30(7):1083–1138, 1994.

[3] Erkorkmaz K. and Altintas Y. High speed cnc system design. part ii: modeling and identification of feed drives. *International Journal of Machine Tools and Manufacture*, 41(10):1487–1509, 2001.

[4] C. Canudas de Wit, H. Olsson, K. J. Astrom, and P. Lischinsky. A new model for control of systems with friction. *Automatic Control, IEEE Transactions on*, 40(3):419–425, 1995.

[5] J. Swevers, F. Al-Bender, C. G. Ganseman, and T. Projogo. An integrated friction model structure with improved presliding behavior for accurate friction compensation. *Automatic Control, IEEE Transactions on*, 45(4):675–686, 2000.

[6] F. Al-Bender, V. Lampaert, and J. Swevers. The generalized maxwell-slip model: a novel model for friction simulation and compensation. *Automatic Control, IEEE Transactions on*, 50(11):1883–1887, 2005.

[7] V. Lampaert. *Modelling and control of dry sliding friction in mechanical systems*. PhD thesis, 2003.

[8] Z. Jamaludin. *Disturbance compensation for machine tools with linear motor drives*. PhD thesis.

[9] H. Olsson, K. J. Åström, C. Canudas De Wit, M. Gäfvert, and P. Lischinsky. Friction models and friction compensation. *European journal of control*, 4:176–195, 1998.

[10] M. Feemster, P. Vedagarbha, D. M. Dawson, and D. Hater. Adaptive control techniques for friction compensation.

[11] C. Canudas de Wit, K. Astrom, and K. Braun. Adaptive friction compensation in dc-motor drives. *Robotics and Automation, IEEE Journal of*, 3(6):681–685, 1987.

[12] A. Kamalzadeh. *Precision control of high speed ball screw drives*. PhD thesis, 2008.

[13] D. Gordon. Precision control of high speed drives using active vibration damping. Master's thesis, 2010.

[14] Y. Hosseinkhani and K. Erkorkmaz. Wide bandwidth control of ballscrew drive using center of mass location feedback.

[15] A. Amthor, S. Zschaeck, and C. Ament. High precision position control using an adaptive friction compensation approach. *Automatic Control, IEEE Transactions on*, 55(1):274–278, 2010.

[16] D. Karnopp. Computer simulation of stick-slip friction in mechanical dynamic systems. *Journal of Dynamic Systems, Measurement, and Control*, 107(1):100–103, 1985.

[17] P. R. Dahl. A solid friction model. Technical report, The Aerospace Corporation, 1968.

[18] P. R. Dahl. Measurement of solid friction parameters of ball bearings. Technical report, The Aerospace Corporation, 1977.

[19] I. D. Mayergoyz. *Mathematical models of hysteresis and their applications*. Academic Press, 2003.

[20] M. A. Krasnoselski and A. V. Pokrovski. *Systems with Hysteresis*. Springer Verlag, 1989.

[21] P. A. Bliman and M. Sorine. Friction modeling by hysteresis operators. application to dahl, sticktion and stribeck effects. In *In Proceedings of the Conference 'Models of Hysteresis'*.

[22] P. A. Bliman and M. Sorine. A system-theoretic approach of systems with hysteresis. application to friction modelling and compensation. In *Proceedings of the 2nd European control conference*, pages 1844–1849, 1993.

[23] P. A. Bliman and M. Sorine. Easy-to-use realistic dry friction models for automatic control. In *Proceedings of 3rd European Control Conference, Rome, Italy*, pages 3788–3794, 1995.

[24] V. Lampaert, J. Swevers, and F. Al-Bender. Modification of the leuven integrated friction model structure. *Automatic Control, IEEE Transactions on*, 47(4):683–687, 2002.

[25] K. Erkorkmaz and Y. Altintas. High speed cnc system design. part iii: high speed tracking and contouring control of feed drives. *International Journal of Machine Tools and Manufacture*, 41(11):1637–1658, 2001.

[26] C. Canudas De Wit, P. Noel, A. Aubin, and B. Brogliato. Adaptive friction compensation in robot manipulators: low velocities. *The International journal of robotics research*, 10(3):189–199, 1991.

[27] J. W. Gilbart and G. C. Winston. Adaptive compensation for an optical tracking telescope. *Automatica*, 10(2):125–131, 1974.

[28] P. Ioannou and B. Fidan. *Adaptive Control Tutorial*. Society for Industrial Mathematics, 2006.

[29] SIEMENS. *Siemens 840D Technical Documentation*. 2009.

[30] I. D. Marinescu, M. Hitchiner, E. Uhlmann, W. B. Rowe, and I. Inasaki. *Handbook of machining with grinding wheels*. CRC Press, 2006.

[31] G. F. Franklin, Powell J.D., and A. Emami-Naeini. *Feedback control of dynamic systems*. PEARSON, 2009.

[32] Pritschow G. A comparison of linear and conventional electromechanical dives. *CIRP Annals-Manufacturing Technology*, 47(2):541–548, 1998.

[33] S. Zschack, S. Buchner, A. Amthor, and C. Ament. Maxwell slip based adaptive friction compensation in high precision applications. In *IECON 2012-38th Annual Conference on IEEE Industrial Electronics Society*, pages 2331–2336. IEEE, 2012.

[34] D. A. Haessig Jr and B. Friedland. Modeling and simulation of friction. In *Orlando'91, Orlando, FL*, pages 383–396. International Society for Optics and Photonics, 1991.

[35] P. Dupont, B. Armstrong, and V. Hayward. Elasto-plastic friction model: contact compliance and stiction. In *American Control Conference, 2000. Proceedings of the 2000*, volume 2, pages 1072–1077. IEEE, 2000.

[36] Qiulin Xie. Modeling and control of linear motor feed drives for grinding machines. 2008.

[37] KAPP. *Siemens 840D user manual*. 2008.